Supplementary Appendix

This appendix has been provided by the authors to give readers additional information about their work.

Supplement to: Liu Y, Jesus AA, Marrero B, et al. Activated STING in a vascular and pulmonary syndrome. N Engl J Med 2014;371:507-18. DOI: 10.1056/NEJMoa1312625

Supplementary Appendix

Activated STING in a vascular and pulmonary syndrome

*Yin Liu, M.D., Ph.D.[1], *Adriana A. Jesus, M.D., Ph.D.[1], *Bernadette Marrero, Ph.D.[1], Dan Yang, M.D.[2], Ph.D., Suzanne E. Ramsey, M.D.[9], Gina A. Montealegre Sanchez, M.D., M.S.[1], Klaus Tenbrock, M.D.[10], Helmut Wittkowski, M.D.[11], Olcay Y. Jones, M.D.[12], Ph.D., Hye Sun Kuehn, Ph.D.[3], Chyi-Chia R. Lee, M.D.[4], Ph.D, Michael A. DiMattia, Ph.D.[1], Edward W. Cowen, M.D.[4], Benito Gonzalez, M.D.[13], Ira Palmer, M.S.[1], John J. DiGiovanna, M.D.[4], Angelique Biancotto, Ph.D.[2], Hanna Kim, M.D.[1], Wanxia L. Tsai, M.S.[1], Anna M. Trier, B.A.[1], Yan Huang, M.D.[1], Deborah L. Stone, M.D.[5], Suvimol Hill, M.D.[6], H. Jeffery Kim, M.D.[7], Cynthia St. Hilaire, Ph.D.[2], Shakuntala Gurprasad, M.T.[3], Nicole Plass, R.N.[1], Dawn Chapelle, R.N.[1], Iren Horkayne-Szakaly, M.D.[12], Dirk Foell, M.D.[11], Andrei Barysenka, Dipl.Phys.[11], Fabio Candotti, M.D.[5], Ph.D., Steven M. Holland, M.D.[8], Jason D. Hughes, Ph.D.[14], Huseyin Mehmet, Ph.D.[14], Andrew C. Issekutz, M.D.[9], Mark Raffeld, M.D.[4], Joshua McElwee, Ph.D.[14], Joseph R. Fontana, M.D.[2], Caterina P. Minniti, M.D.[2], Susan Moir, Ph.D.[8], Daniel L. Kastner, M.D.[5], Ph.D., Massimo Gadina, Ph.D.[1], Alasdair C. Steven, Ph.D.[1], Paul T. Wingfield, Ph.D.[1], Stephen R. Brooks, Ph.D.[1], Sergio D. Rosenzweig, M.D.[3], Ph.D., Thomas A. Fleisher, M.D.[3], *Zuoming Deng, Ph.D.[1], *Manfred Boehm, M.D.[2], *Amy S. Paller, M.D.[15], and Raphaela Goldbach-Mansky, M.D., MHS.[1]

*These first three authors Y.L., A.A.J. and B.M. contributed equally to this work; and Z.D., M.B. and A.S.P. contributed equally.

[1]National Institute of Arthritis and Musculoskeletal and Skin Diseases, NIH, Bethesda, MD; [2]National Heart, Lung, and Blood Institute, NIH, Bethesda, MD; [3]Department of Laboratory Medicine, NIH, Bethesda, MD; [4]National Cancer Institute, NIH, Bethesda, MD; [5]National Human Genome Research Institute, NIH, Bethesda, MD; [6]Department of Radiology and Imaging Services, NIH, Bethesda, MD; [7]National Institute of Deafness and Other Communication Disorders, NIH, Bethesda, MD; [8]National Institute of Allergy and Infectious Disease, NIH, Bethesda, MD; [9]Dalhousie University, Halifax, Canada; [10]RWTH Aachen University, Aachen, Germany; [11]University Hospital of Muenster, Muenster, Germany; [12]Walter Reed National Military Medical Center, Bethesda, MD; [13]Luis Calvo Mackenna Hospital, Santiago, Chile; [14]Merck Research Laboratories, Boston, MA; [15]Northwestern University Feinberg School of Medicine, Chicago, IL

CONTENTS

III. Supplementary Tables

I. Supplementary Methods

1. PATIENTS

All adult patients or parents of minor patients and family members gave written informed consent for genetic testing and participation. Parents of deceased patients were contacted for permission to include archived data.

2. GENETIC STUDIES

Whole Exome Sequencing

Agilent SureSelect® Human 51 Mbp All Exon Kit (Agilent Technologies, Santa Clara, CA) was used for exome capture. Sequencing was performed on Illumina® HiSeq sequencers (Illumina, San Diego, CA) using 2x100 bp paired reads. The typical average on-target coverage is about 120X. A computational pipeline was developed to process the read data and perform tasks such as quality control (QC), variant discovery, annotation and filtering. Briefly, the sequencing reads in FASTQ format were aligned to the human reference genome (GRC B37) with the BWA (Burrows-Wheeler Aligner) mapping tool. The resulting BAM files (one per sample) were further processed to remove duplicate reads, refine alignment around indels and recalibrate base quality scores, according to the best practice guideline by the Genome Analysis Toolkit (GATK) from the Broad Institute. A variant caller (UnifiedGenotyper) from GATK was used to make joint variant calls across multiple samples, followed by a variant quality score recalibration step by the GATK VQSR tool. Besides quality scores, the variants were annotated with functional impact and allele frequency in public databases and local datasets. Sample relationship and gender were checked to identify potential sample mix-up and false family relationship. Likely disease-causing mutations were selected and prioritized based on quality score, allele frequency, functional impact, probable inheritance model (de novo mutation**,** autosomal recessive, autosomal dominant, or X-linked), and expert evaluation.

Sanger Sequencing

The reference sequence used for primer design and nucleotide numbering was *TMEM173* (NM_198282). The exonic regions and flanking intronic sites of the gene were amplified by polymerase chain reaction (PCR) using specific primers (IDT, Coralville, IA) designed with *Exon Primer* (http://ihg.gsf.de/ihg/ExonPrimer):

Exon	Primers sequence Forward (above) Reverse (below)	PCR product size (bp)
Exon 3	CAGAGCCTCAGTCCCAGAAG	351
	CATCAAGGGAGTGACACACG	
Exon 4	CCCTCCTTGAACCTCTCTGG	319
	CTCAGGGCAGGTCACACC	
Exon 5	CAGGAGGAGGAGTTCTCTGGG	242
	AACACAAGAGGCTGTGTGTCTTAG	
Exon 6	GAATCAGGTGGGAGATAGGG	239
	TTCATCAGTGCTTGGCTAGG	
Exon 7	GACCCTCCATTCTCCATCC	327
	ACTCTTTGGGAGACCCTGG	
Exon 8	TATGTTTGAGTGGGAATGGG	333
	GGACATTCAGCCACTGAAGAG	

The first PCR amplification reaction was performed in a final volume of 13 μl containing 1 μl (10 μM) of each primer, 6 μl of GoTaq® Hot Start Master Mix (Promega, Madison, WI) and 20-200 ng of template DNA. The reactions were carried out for 35 cycles: denaturation at 94°C for 30 seconds, annealing at 60°C for 30 seconds, extension at 72°C for 1 minute. After the PCR, the DNA fragments were treated with Exo-Sap (GE Healthcare Bioscience, Pittsburgh, PA) for clean up. PCR products underwent a second PCR reaction with ABI Prism® BigDye Terminator v1.1 Cycle Sequencing Kit (Applied Biosystems, Foster City, CA) and directly sequenced in both directions using ABI 3100 Genetic Analyzer (Applied Biosystems). Results were analyzed using *DNAStar Lasergene* software. *TMEM173* variant detected by WES in Patient 1 (N154S) was confirmed by targeted sequencing of exon 5. Targeted sequencing of the 6 coding exons of *TMEM173* was performed for the detection of mutations in Patients 2 to 6.

3. FUNCTIONAL STUDIES FROM PATIENTS' SAMPLES

Gene-Expression Analysis by RNA_Sequencing (RNA_Seq)

Total RNA was extracted from blood samples of Patients 1, 3, 4 and 6 collected in PaxGene tubes (Qiagen, Valencia, CA). RNA integrity was analyzed with Agilent 2100 Bioanalyzer. mRNA purification and fragmentation, complementary DNA synthesis and target amplification were performed using the Illumina® TruSeq RNA Sample Preparation Kit (Illumina). Pooled cDNA libraries were sequenced using HiSeq 2000 Illumina® platform (Illumina). Sequencing results were expressed in RPKM (reads per kilobase exon per million mapped). Hierarchical clustering was conducted with the use of Partek software (version 6.6). Patients and healthy controls were compared using Anova analysis and a list of the 2-fold up- or downregulated genes was generated. Statistical significance level adopted was $p<0.05$. Gene lists were uploaded into Ingenuity Pathway Analysis (http://www.ingenuity.com) in order to determine the differentially regulated canonical pathways in the patients. Results for IFN-regulated genes are shown as a heat map, with shades of red denoting upregulated genes and shades of blue denoting downregulated genes.

Cytokine Analysis

Serum was collected from Patients 1, 3, and 4 and stored at -80°C. The concentrations of 48 cytokines were measured in serum samples from both the patients and controls using the Bio-Plex Pro™ Human Cytokine 27-Plex and 21-Plex Immunoassays (Bio-Rad, Hercules, CA) according to the manufacturer instructions. Human cytokine standard group I and II were used for the standard curves. The sera were diluted 1:4 with the sample buffer and 50 µl of the diluted serum were used for the assays.

qRT-PCR Quantification of Gene Expression

PBMCs, fibroblasts and human umbilical vein endothelial cells (HUVEC) were stimulated as described below. Total RNA was extracted by using TRIzol (Life Technologies, Grand Island, NY). Reverse transcription was done using the High-Capacity cDNA Reverse Transcription Kit (Applied Biosystems). IFNβ encoding gene (*IFNB1*) or other messenger RNAs were quantified by qRT-PCR using Taqman Gene Expression Assay (Applied Biosystems) and normalized against 18S gene expression.

Analysis of STING Protein Expression and IRF3 Phosphorylation

Cell lysate was made from PBMCs, purified neutrophils, flow cytometer sorted monocytes, NK cells, T cells, B cells, cultured skin fibroblasts and endothelial cells by using RIPA buffer (Cell Signaling, Danvers, MA) supplemented with 1 mM PMSF and protease inhibitor cocktail (Roche Mannheim, Germany). Protein concentration was determined with the BCA Protein Assay Kit (Pierce-Thermo Scientific, Pittsburg, PA). For analysis of STING expression and

IRF3 phosphorylation, 10-15 μg of lysate was resolved in a 4-12% NuPAGE Tris Bis gel under reducing and denaturing condition and transferred to nitrocellulose membranes. The membranes were blocked with either 5% milk or odyssey blocking buffer (LI-COR, Lincoln, NE), blotted with anti-STING Ab (1:1000 R&D systems, Minneapolis, MN) or anti-pIRF3 Ab (1:1000, Cell Signaling) followed by the IRDye secondary Abs (800CW and 680RD LI-COR). The membrane was scanned with an Odyssey Scanner (LI-COR). Relative fluorescence intensity of the bands was analyzed using the Image Studio Lite software (LI-COR). Protein levels are expressed in the graph as arbitrary fluorescent units quantifying pixel intensities from samples normalized to their housekeeping gene such as beta actin or alpha tubulin.

Peripheral Blood Mononuclear Cells (PBMC), Fibroblasts and Endothelial Cells Stimulation Assays

For PBMCs stimulation, $1x10^6$ PBMCs from either Pt.1, Pt.3, Pt.6 or healthy controls were resuspended in 1 ml complete medium (10% FBS RPMI1640). cGAMP was added to the culture medium directly at indicated concentration and 24 hours later, RNA was extracted from the cells with TRIzol. qRT-PCR analysis for gene expression was done as described.

For fibroblasts stimulation, $2x10^5$ fibroblasts from Pt.1, Pt.3 and various controls were seeded into 6 well plate 24 hours before experiment. cGAMP stimulation was carried out through digitonin delivery as described (Science. 2010 Jun 25;328(5986):1703-5). Briefly, cGAMP at various concentrations were mixed with digitonin permeabilization solution (50 mM HEPES pH 7.0,100 mM KCl, 3 mM $MgCl_2$, 0.1 mM DTT, 85 mM Sucrose, 0.2% BSA, 1 mM ATP, 10 μg/mL Digitonin). Culture medium was removed from the cells, and 1ml of digitonin permeabilization solution, with or without cGAMP, was added to the cells and incubated in 37°C incubator for 25 minutes. After removing the buffer, 2 ml complete culture medium was added to the cells and culture continued until 4 hours after stimulation. RNA was extracted from the cells with TRIzol. qRT-PCR analysis or RNA_seq was done as described.

For Human Umbilical Vein Endothelial Cell (HUVEC) stimulation, cells at passage 2-6 were plated on 6-well plate 200,000 cells per well. The next day, cells were stimulated or not with 5 μg/ml or 20 μg/ml cGAMP for 24 hours. RNA was extracted from the cells with TRIzol. qRT-PCR analysis or RNA_seq were done as described.

Human Monocytes Culture and Differentiation

PBMCs were isolated from whole blood by centrifugation through Ficoll-Paque plus solution (GE healthcare Bio-Sciences AB) and washed twice in PBS. Monocytes were purified from PBMCs by negative selection (Monocyte Isolation Kit II; Miltenyi Biotec). Monocytes were seeded at a density of 150,000 cells/cm^2 and cultured in RPMI 1640 (Gibco) supplemented with 10% FBS, 2 mM L-glutamine, penicillin (100 U/ml), and streptomycin (100 μg/ml). Primary human monocytes were differentiated into macrophages using 50 ng/ml human macrophage colony-stimulating factor (hM-CSF, Sigma) or 20 ng/ml human Granulocyte-macrophage colony-stimulating factor (GM-CSF, Sigma) for 10-16 days. Media were changed every 2-3 days.

STAT Phosphorylation Assay

1. Method used: PBMCs were either left unstimulated or stimulated with indicated cytokines (IL-2 (100 U/ml), IL-4, IL-6, IL-7 (10 ng/ml), IL-15, IL-21 (50 ng/ml), IFNα (5 ng/ml)) for 15-20 minutes with CD4-APC or CD8-Pacific blue surface marker at 37°C. Cells were fixed using BD Cytofix Fixation Buffer (10 minutes at 37°C) and then permeabilized in BD Phosflow Perm Buffer III (30 minutes on ice). Cells were then washed twice with PBS, and stained with indicated phospho-STAT antibody for 1 hour. The cells were analyzed on a BD FACSCanto II flow cytometer.

2. Method used: Ficolled PBMCs were resuspended in 1% FBS PBS and left in 37°C incubator for 4 hours in the presence or not of 1 μM tofacitinib, 100 nM ruxolitinib or 200 nM baricitinib. At the last half hour of the incubation, the cells were stimulated or not with IFNα (30 minutes), IL-6

or IL-7 (20 minutes). The stimulation was terminated by adding equal volume of 4% PFA to each sample and incubated at room temperature for 15 minutes. After washing two times, the cells were permeabilized with 1 ml cold methanol and left on ice for 15 minutes. The cells were then washed three times and stained for pSTAT Alexa647 (anti-STAT1 pY701 for cells stimulated with IFNα; anti-STAT3 pY705 for cells stimulated with IL-6 and anti-STAT5 pY694 for cells stimulated with IL-7) and cell surface makers (CD14.Brilliant Violet 421, CD4.Alexa 488, CD19.PE and CD8.PercpCy5.5). Flow cytometric analysis was performed using a FACSCanto system (BD Biosciences). Results were analyzed using FlowJo software (TreeStar). The first experiment on Patient 3 was performed by as described in Method 1. However, because of cell loss during the staining procedure and difficulties in staining of B cell markers, we then switched to Method 2.

Apoptosis Assays

Staining active caspase-3: PBMCs from patients and controls were isolated by Ficoll density gradient centrifugation, resuspended in 10% FBS RPMI1640 and cultured in a 37^{o}C incubator for 4 hours. Staining of active caspase-3 as an indication of apoptosis was done using the CaspGlow Fluorescein Active Caspase-3 Staining Kit (eBioscience, Affymetrix, San Diego, CA), following the recommended procedure. At the end of the assay, cell surface marker staining was done at room temperature for 15 minutes. Flow cytometer analysis was performed using FACSCanto (BD Biosciences).

4. TRANSFECTION STUDIES IN HEK293T cells

Generation of *TMEM173* Mutations

Human *TMEM173* cDNA in a pSPORT6 expression vector was purchased from Open Biosystems (RefSeq: NM_198282). The reference sequence obtained carries a histidine at amino acid position 232, which represents a less common haplotype. We mutated the histidine to an arginine, which represents the most prevalent haplotype (PLoS One. 2013 Oct 21:8(10):e77846), and we refer to both H232 and R232 backgrounds as wildtypes in the paper. We generated constructs with all mutations (N154S, V155M, V147L and V155R) on the background of R232 and H232 haplotypes. Mutations were introduced by using the Quikchange Site-Directed Mutagenesis Kit (Agilent Technologies). All mutant constructs were fully sequenced.

***IFNB1* Luciferase Reporter Assay**

Transfection in HEK293T cells was done using the Lipofectamine 2000 transfection reagent (Life Technologies). Briefly, HEK293T cells were seeded into 24 well plates at 125,000 cells per well 24 hours before transfection in 10% FBS DMEM media (Life Technologies) supplement with 2 mmol/L L-glutamine, penicillin (100 U/ml) and streptomycin (100 μg/ml). Immediately prior to transfection, media was changed to 200 µl Opti-MEM (Life Technologies). 2 µl Lipofectamine and indicated amount of plasmids (STING constructs, *IFNB1* firefly luciferase reporter construct and Renilla luciferase construct) were each diluted in 50 µl Opti-MEM media, mixed and incubated at room temperature for 30 minutes. The transfection mixture was then added to the cells dropwise. After four hours, 1 ml of complete media 10% FBS DMEM was added and cells were continuously cultured for 24 hours. 4 hours prior to reporter assay, the cells were stimulated or not with cGAMP by digitonin delivery through the same procedure described above for fibroblast stimulation. Luciferase activity was analyzed by using the Dual-glo Luciferase assay system kit (Promega) and the Firefly luciferase reporter activity was normalized against the Renilla luciferase activity for control of transfection efficiency.

5. TISSUE STAINING

Immunohistochemistry
Skin biopsy tissue was obtained for diagnostic purposes. Healthy control skin and lung tissues were obtained through the NIH pathology department. Paraffin-embedded skin biopsy samples from Patients 2 and 3 and healthy control individuals were deparaffinized with four sequential washes in xylene (8 minutes each), followed by two washes for 1 minute each in 100% ethanol, and a series of 1 minute washes each in 90%, 80%, 70%, and 50% ethanol. Slides were then rinsed with water. Antigen retrieval was done by using the Diva Decloaker buffer (Biocare, Concord, CA) at 95°C for 30 minutes. The tissue slides were blocked with 1x Cassine buffer (Vector) at room temperature for 1 hour. Rabbit antibodies against STING (1:150, Sigma) were added overnight at 4°C, followed by the Polink-2 Plus 2-step polymer detection kits (Golden Bridge International) following the recommended procedures.

Tissue Immunofluorescence Staining
For staining on formalin-fixed, paraffin-embedded skin samples, slides were deparaffinized with two 30 minutes washes in xylene, followed by two 100% ethanol washes for 1 minute each, and a series of 1 minute washes in 90%, 80%, 70% and 50% ethanol. Slides were then rinsed with water. Antigen retrieval was performed in a solution of 10 mM sodium citrate, pH 6.0 for 40 minutes at 95°C. After cooling completely, samples were blocked for one hour in 5% BSA, 20% donkey serum in PBS with 0.1% Triton-X100. Primary antibodies for CD31 (1:50, DAKO), STING (1:100, Sigma), iNOS (1:100, Abcam), Tissue Factor (TF, 1:50, Abcam), E-selectin (1:25, Abcam), ICAM-1 (Abcam, 1:50) and vWF (1:200, DAKO) were applied overnight at 4°C, followed by the corresponding secondary antibody for 1 hour at RT. Slides were mounted using DAPI-containing mounting media (Vector Laboratories). Slides were imaged using a confocal microscope (Zeiss LSM 510 META) at the stated magnification.

6. ENDOTHELIAL CELL EXPERIMENTS

Human Primary Dermal Microvascular Endothelial Cells (HMVEC) Culture and Immunofluorescence Staining
HMVEC (Lonza) were maintained in EGM2 growth media (Lonza). Passage 2-5 cells were used for experiments. Cells were treated with or without 20 μg/ml cGAMP (Invitrogen) for 24 hours. Cells were fixed with 4% paraformaldehyde for 10 minutes at RT. The primary antibody VE-Cadherin (1:200, Enzo) and iNOS (1:50, Abcam) were applied overnight at 4°C, followed by the corresponding secondary antibody for one hour at RT. DAPI (1:1000) was used for cell nuclei detection. Cells were imaged using a Nikon Eclipse TE300 inverted fluorescence microscope. Three replicates were performed for every observation.

Stimulation assays with Human Umbilical Vein Endothelial Cells (HUVEC) are described in section 3, under Peripheral Blood Mononuclear Cells (PBMC), Fibroblasts and Endothelial Cells Stimulation Assays.

7. STING PROTEIN ANALYSES AND EXPRESSION

In Silico Modeling
Molecular graphics were produced using PyMOL (DeLano Scientific LLC) with PDB accession IDs 4EF5 and 4KSY.

Recombinant Expression and Purification of STING and Mutational Variants

Wildtype his-tagged STING and the two disease causing mutant variants (N154S and V155M) were expressed in *E. coli.* All proteins exhibited high levels of expression: about 50% of the wildtype protein was soluble whereas neither N154S nor V155M were soluble. The soluble portion of the wildtype showed significant protease cleavage in the cell lysate; hence, all proteins were purified and refolded from the insoluble cell fractions. Firstly, proteins were extracted and solubilized with 4 M guanidine-HCl, and purified using a Ni-Sepharose column followed by gel filtration using a Sephadex S200 column. Both columns were run in the presence of guanidine-HCl. The proteins were folded by dialysis against 4 M urea and then stepped through lower concentrations until the urea was removed. Reductant was present in all buffers to prevent artefactual disulfide bond formation during folding.

Analytical Ultracentrifugation

Analytical ultracentrifugation was carried out using a Beckman Optima XL-I analytical ultracentrifuge. Absorption optics, an An-60 Ti rotor, and standard double-sector centerpiece cells were used. Equilibrium measurements at 20°C were made after 16 h at 16,500 rpm. A baseline was established by overspeeding at 45,000 rpm for 3 h. Data (the average of five scans collected using a radial step size of 0.001 cm) were analyzed using the standard Optima XL-I data analysis software. Protein partial specific volumes were calculated from amino acid compositions and a value of 0.728 mL/g was used for all proteins.

II. Supplementary Figures

Supplementary Figure S1. Clinical lesions in patients with SAVI

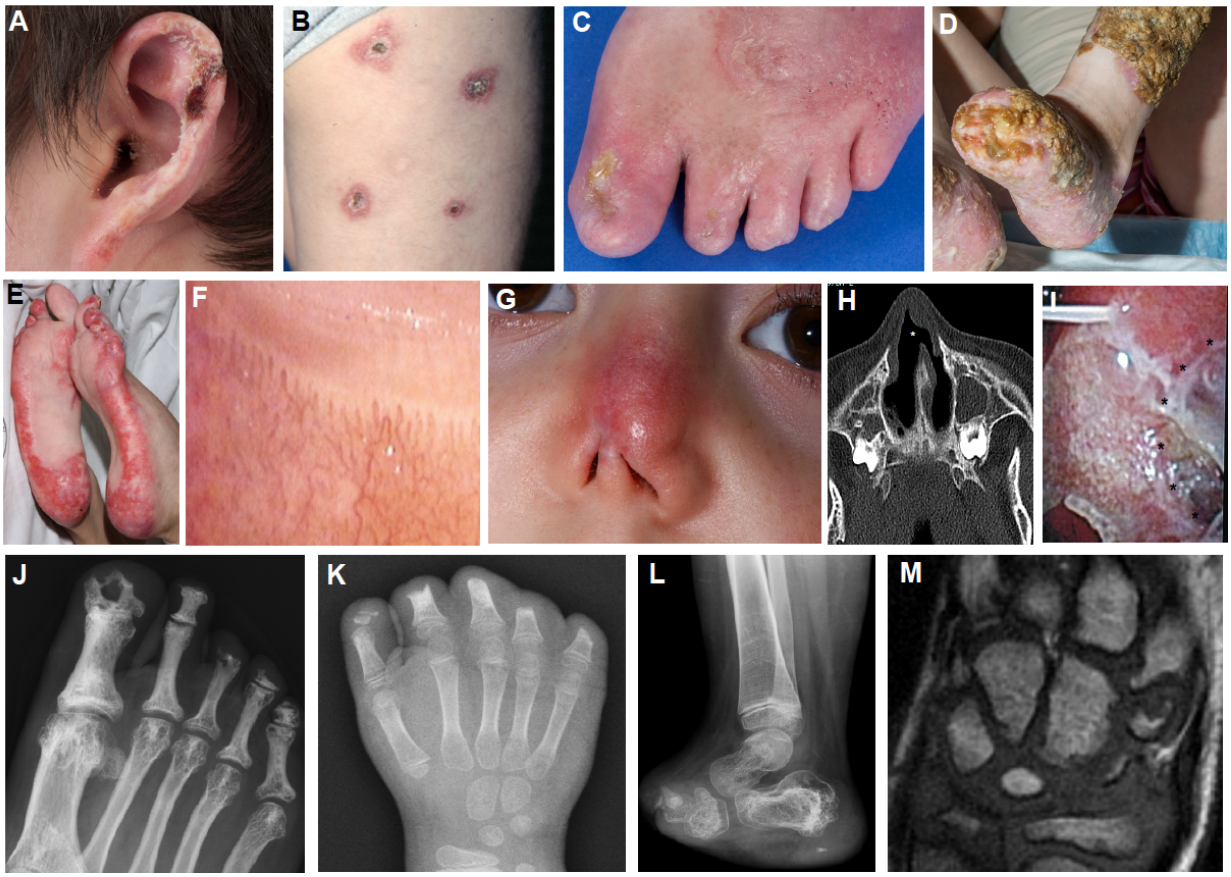

Panel A shows ulcerated lesions on the pinna of the ear with scales and crusts (Pt.6). **Panel B** shows punched out ulcerations with central eschars that are surrounded by violaceous erythema (Pt.2) and **Panel C** depicts erythematous, scaling plaques with atrophy and scarring of the dorsal aspect of the foot and toes with digital swelling, acral tissue loss and nail dystrophy (Pt.6). **Panel D** depicts extensive eschar formation overlying non-healing wounds that are secondarily infected after surgical amputation (Pt.3). **Panel E** shows violaceous, and atrophic plaques on feet of Pt.5. **Panel F** shows tortuous and thickened capillary nail folds with capillary loop loss (Pt.2). **Panel G** shows telangiectasia, atrophy and scarring of the skin with loss of deep tissue of the nose following an inflammatory lesion (Pt.5). **Panel H** depicts a computed tomography (CT) of the sinuses revealing a septal defect (white star) and **Panel I** shows a picture taken when the right nostril was examined showing the septal perforation at 3o'clock (indicated by black stars) (Pt.6). **Panel J** shows an oblique view of the right foot demonstrating resorption of distal phalanges and partial bony ankylosis of the right 1st distal interphalangeal joint (Pt.6). **Panel K** depicts a right hand x-ray showing the sites of surgical amputation at the proximal phalanges level of the 2nd to the 5th fingers and 1st distal phalanx (Pt.4). **Panel L** shows a left foot x-ray after surgical amputation at the level of the tarsal bones in Pt.4. **Panel M** shows carpal erosions in Pt.5 with seropositive erosive rheumatoid arthritis.

Supplementary Figure S2. Histopathology of vascular lesions in SAVI patients

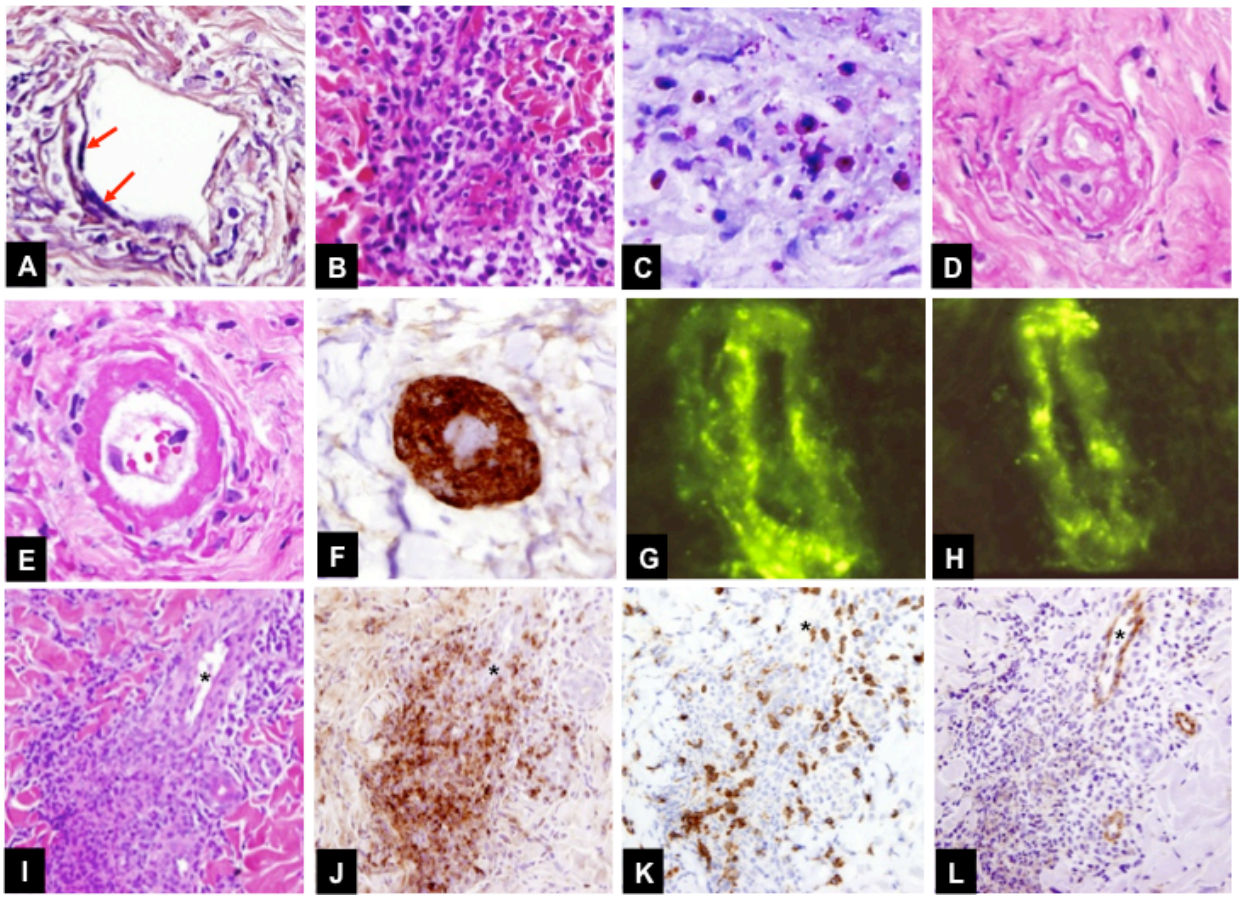

Panels A to D depict progression of small vessel vasculitis to destruction of the vessel. **Panel A**. The earliest lesion in undestroyed vessels is deposition of fibrin, here visualized in a small superficial dermal vessel using a Phosphotungstic Acid Hematoxylin (PTAH) stain for fibrin. Fibrin deposition on the vascular wall is marked with red arrows. **Panel B**. A dense inflammatory infiltrate surrounding a severely damaged vessel is depicted. In **Panel C** the dense inflammatory infiltrate was further characterized using a chloroacetate esterase (Leder) stain, which confirms the presence of neutrophil precursors with karyorrhectic debris. **Panel D** shows a completely destroyed and occluded blood vessel with fibrin deposits. **Panel E** shows fibrinoid necrosis of the vessel wall stained by hematoxylin and eosin (H&E). **Panel F** depicts dense IgM deposits in a vessel wall of a histologically comparable vessel stained by immunoperoxidase using an anti-IgM antibody. Direct immunofluorescence (DIF) performed on fresh tissue revealed granular IgM (**Panel G**) and complement factor 3 (C3) deposits in a vessel wall (**Panel H**). **Panels I to L** show contiguous slides of small vessel vasculitis (vessel marked with asterisk) characterized by a dense inflammatory infiltrate composed of predominantly neutrophils with karyorrhexis and damage to the vessel wall (Original magnification, 400x) (**Panel I**). Myeloperoxidase immunohistochemical staining showed a dense neutrophilic inflammatory infiltrate surrounding a small blood vessel (**Panel J**); CD3 immunohistochemical staining showed scattered T-lymphocytes around a blood vessel (**Panel K**); and CD31 immunohistochemical staining highlighted endothelial cells of the affected blood vessel, some with non-contiguous staining indicative of vascular damage at the pole of neutrophil infiltration (**Panel L**). (Photographs taken at 600x original magnification unless differently specified in the text).

Supplementary Figure S3. Histopathology of lung and muscle lesions in SAVI patients

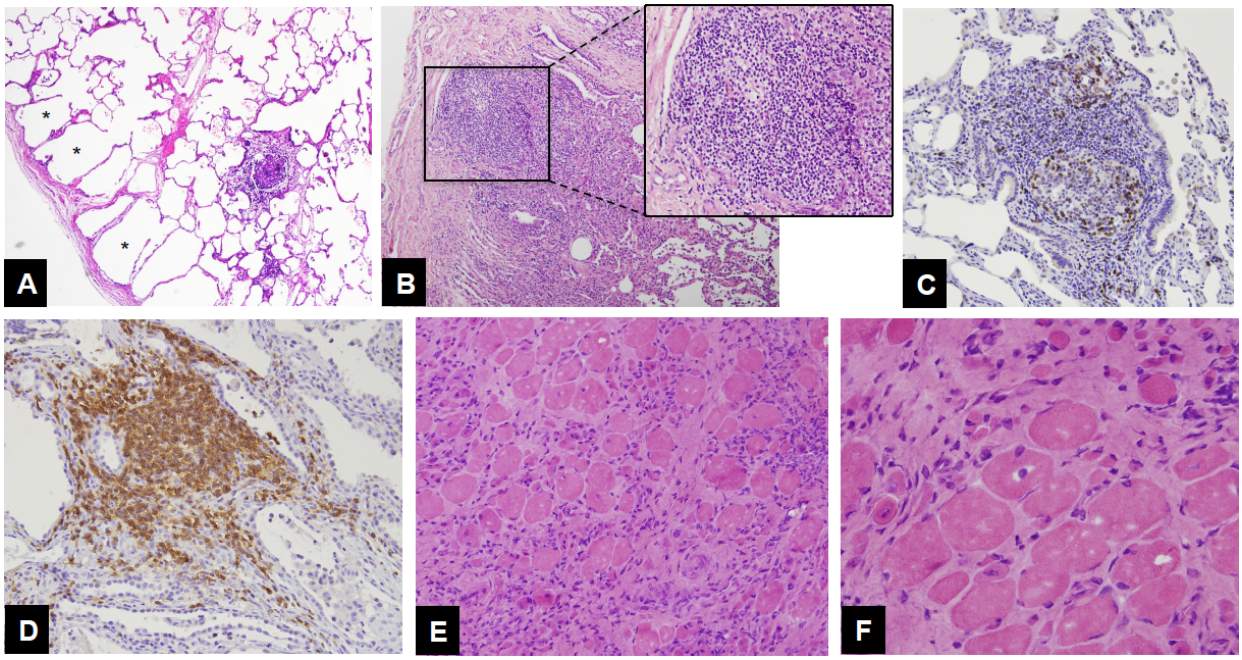

Panels A to C. Lung tissue from Patient 1. **Panel A** depicts a lymphoid aggregate within the lung parenchyma. There are emphysematous changes in some alveolar spaces (*). **Panel B**. Lung biopsy tissue shows a patchy interstitial lymphoid infiltrate in the lung parenchyma (Original magnification 100x). **Panel C**. CD3 immunohistochemistry depicts a few scattered T-lymphocytes within the interstitial lymphoid aggregate (Original magnification 200x). **Panel D**. CD20 immunohistochemistry shows a predominant population of B-lymphocytes within the interstitial lymphoid follicles. (Original magnification 200x). **Panels E and F.** Muscle tissue from Pt.5. **Panel E**. Cross sections of a skeletal muscle biopsy specimen show a moderately dense lymphocytic inflammatory infiltrate and fibrosis between the skeletal muscle fibers (Original magnification 200x). **Panel F**. Higher magnification of muscle biopsy revealed atrophy and regeneration of skeletal muscle fibers (Original magnification 400x).

Supplementary Figure S4. Whole exome sequencing and electropherograms of patients with SAVI and their parents identifying *de novo TMEM173* mutations

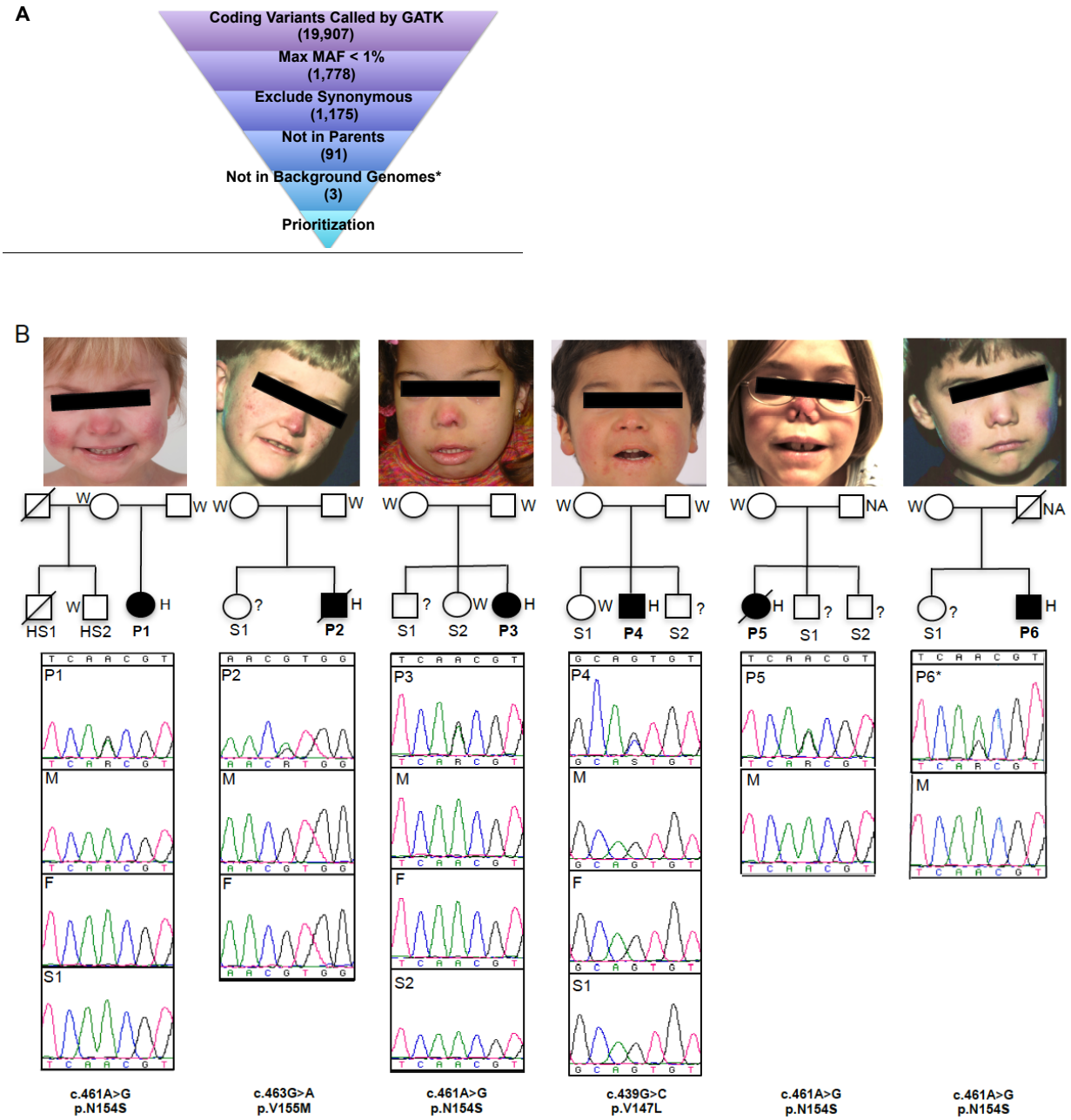

Panel A shows the whole exome sequencing (WES) filtering performed for Patient 1 and her parents. **Panel B**. The pedigrees of the six children with mutations in *TMEM173* are presented. Solid symbols indicate Patients 1 through 6, open symbols unaffected relatives, squares male subjects, circles female subjects, and slashes deceased individuals. W denotes wildtype; NA denotes DNA was not available for genetic testing; P denotes patient; S denotes sibling; HS denotes half-sibling; M denotes mother; F denotes father; question mark (?) denotes unknown genotype; *Pt.6 possibly harbors a somatic mutation and the electropherogram shown is the sequencing result of DNA extracted from neutrophils.

Without paternal samples we could not “prove” that the mutation occurred *de novo* in Pt.5 and Pt.6. However this variant has not been reported in any of the searched databases (Table S3 of the Supplementary Appendix).

Supplementary Figure S5. Sequencing of different tissue samples suggests that the mutation in Patient 6 may be of somatic origin

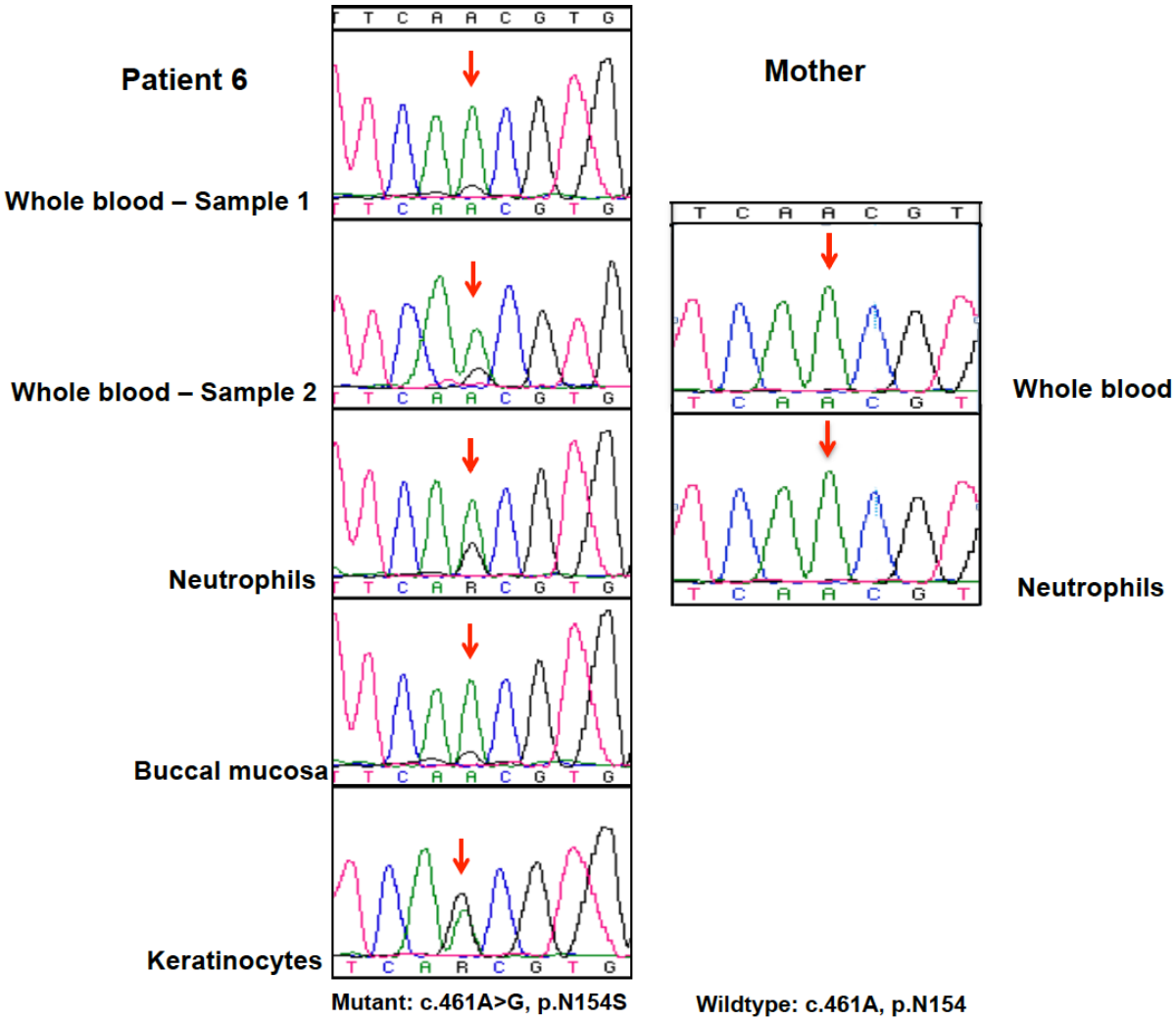

To investigate whether the mutation occurred *de novo* in a somatic cell, we sequenced sorted blood subsets, buccal mucosa cells and primary dermal keratinocytes obtained from a skin biopsy. Sequencing of the different cell subsets suggests that Pt.6 harbors a somatic mutation in *TMEM173* that is present in the highest copy number in keratinocytes, followed by neutrophils and in lower copy numbers in blood and buccal mucosa cells. The presence of the mutation in primary keratinocyte cell lines and in buccal mucosa, which are of ectodermal origin, and in blood cells, which are of mesodermal origin, suggest that a somatic mutation likely occurred in a pluripotent cell precursor prior to differentiation into ectoderm, mesoderm and endoderm and further experiments to understand the origin of the mutation are planned.

Supplementary Figure S6. Protein domains and multi-species alignment of STING

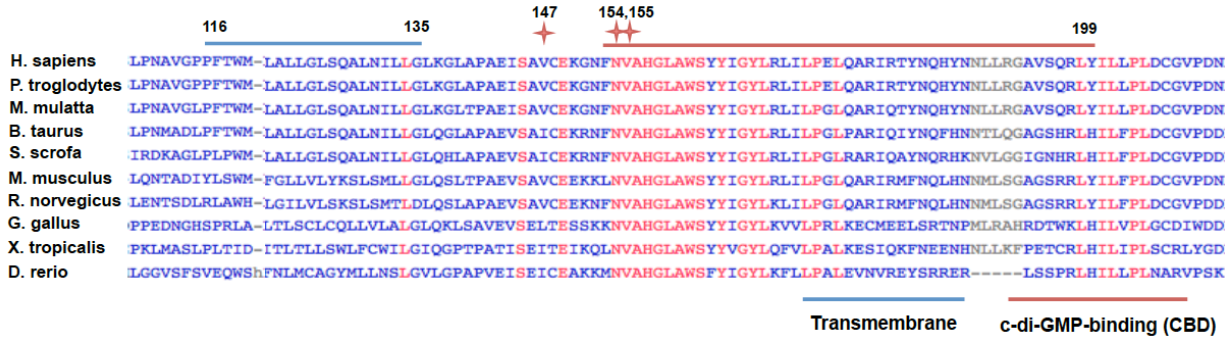

The position of the 3 mutations described in the 6 patients with SAVI are shown (red stars). Mutations N154S and V155M are located in the c-di-GMP-binding domain (CBD) of the protein and mutation V147L is located 6 amino acids (AA) apart from this domain. The conservation of the AAs mutated is depicted at positions 147, 154 and 155 of STING protein. Whereas the AAs at positions 154 (asparagine) and 155 (valine) are highly conserved among various species, the AA affected by the *de novo* mutation at position 147 in Pt.4 is not conserved and is either a valine (human, *Homo sapiens*; common chimpanzee, *Pan troglodytes*; Rhesus macaque, *Macaca mulatta*; mouse, *Mus musculus*; and brown rat, *Rattus norvegicus)* or an isoleucine (cow, *Bos taurus*; wild boar, *Sus scrofa*; western clawed frog, *Xenopus tropicalis*; and zebrafish, *Danio rerio*) in most of the species. In chicken, *Gallus gallus*, the amino acid identified at position 147 is a leucine.

Ref: Biacchesi S, Mérour E, Lamoureux A, Bernard J, Brémont M. Both STING and MAVS fish orthologs contribute to the induction of interferon mediated by RIG-I. PLoS One. 2012;7:e47737.

Supplementary Figure S7. Recombinant protein expression and testing for dimerization of wildtype and mutant protein

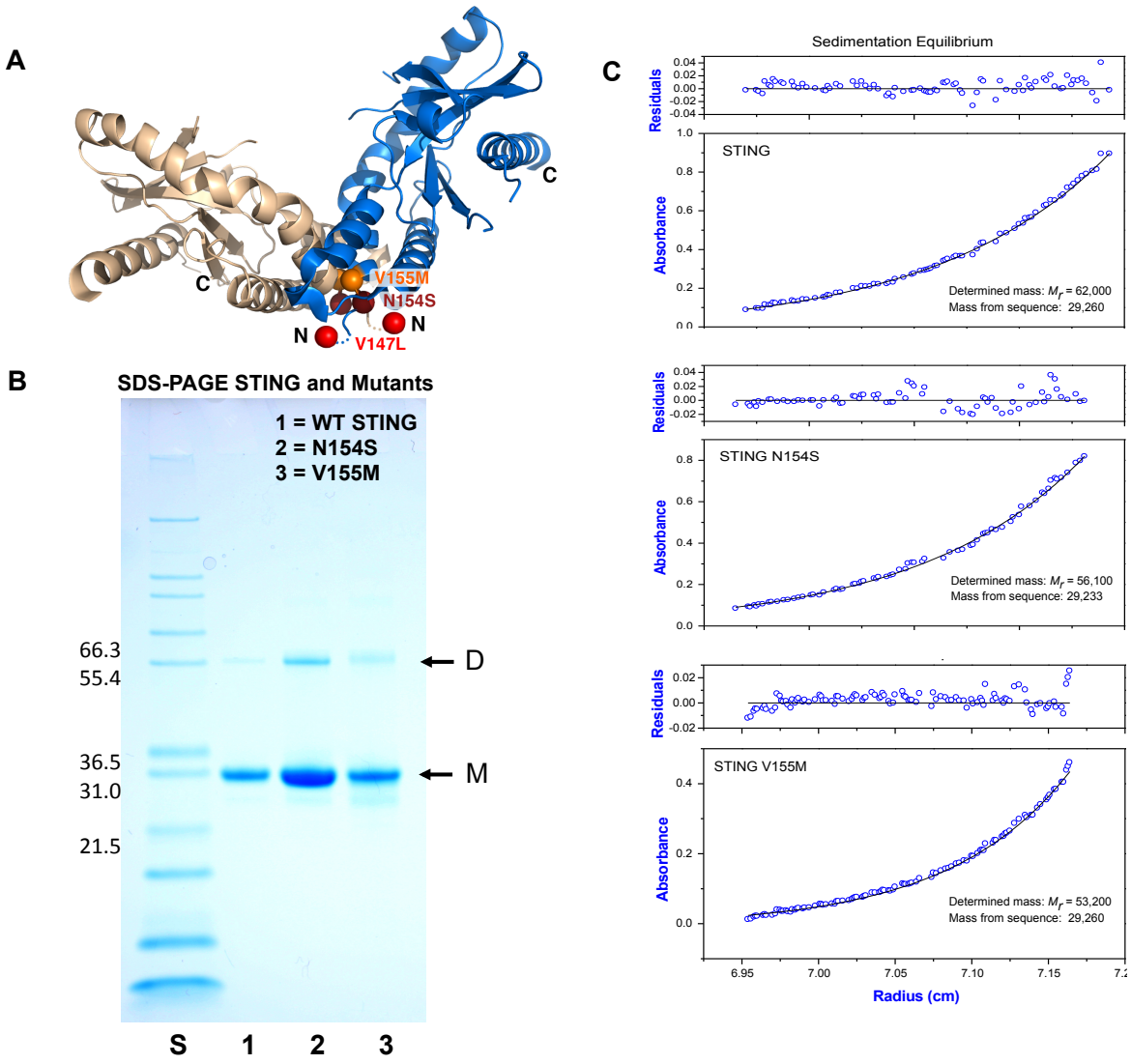

Panel A shows a ribbon representation of the STING dimer in "open" conformation (PDB ID: 4EF5). The dimer subunits are colored in wheat and blue, respectively. Two of the mutations, N154S (dark red), and V155M (orange) are located at the dimerization interface. V147L (red) is located in the adjacent disordered region. **Panel B** refers to SDS-PAGE of STING WT and the two single site mutants STING N154S and STING V155M. All proteins were purified and folded from *E.coli.* They have molecular weights of ~ 29,000 (M) with small amounts of dimer (D) under denaturing conditions. **Panel C** refers to the direct determination of the molecular weights of STING and variants under native conditions by sedimentation equilibrium. For each panel the bottom section is absorbance at 280 nm and the upper section is residuals. Open circles show UV absorbance gradients in the centrifuge cell. The solid line indicates the calculated fit for an ideal single species. Residuals show the difference in the fitted and experimental values as a function of radial position (a random distribution is diagnostic of a good fit). For each protein, comparison of the DNA derived molecular weight (equivalent to a monomeric molecular weight) with the experimentally determined molecular weights (M_r) indicates that the latter values are close to twice that of the former indicating that the proteins

are dimeric. The deviations from exact dimeric estimations are within the (+/-) 5% accuracy of the method and potential error from inclusion of DTT in the buffers. Diagnostic analyses of the protein concentration gradients shown in B support the view that the dimers are stable entities, for example, not in equilibrium with monomeric protein as would be for reversible monomer-dimer systems.

Supplementary Figure S8. Expression of STING in blood cells and fibroblasts and transcription of biomarkers in peripheral blood cells

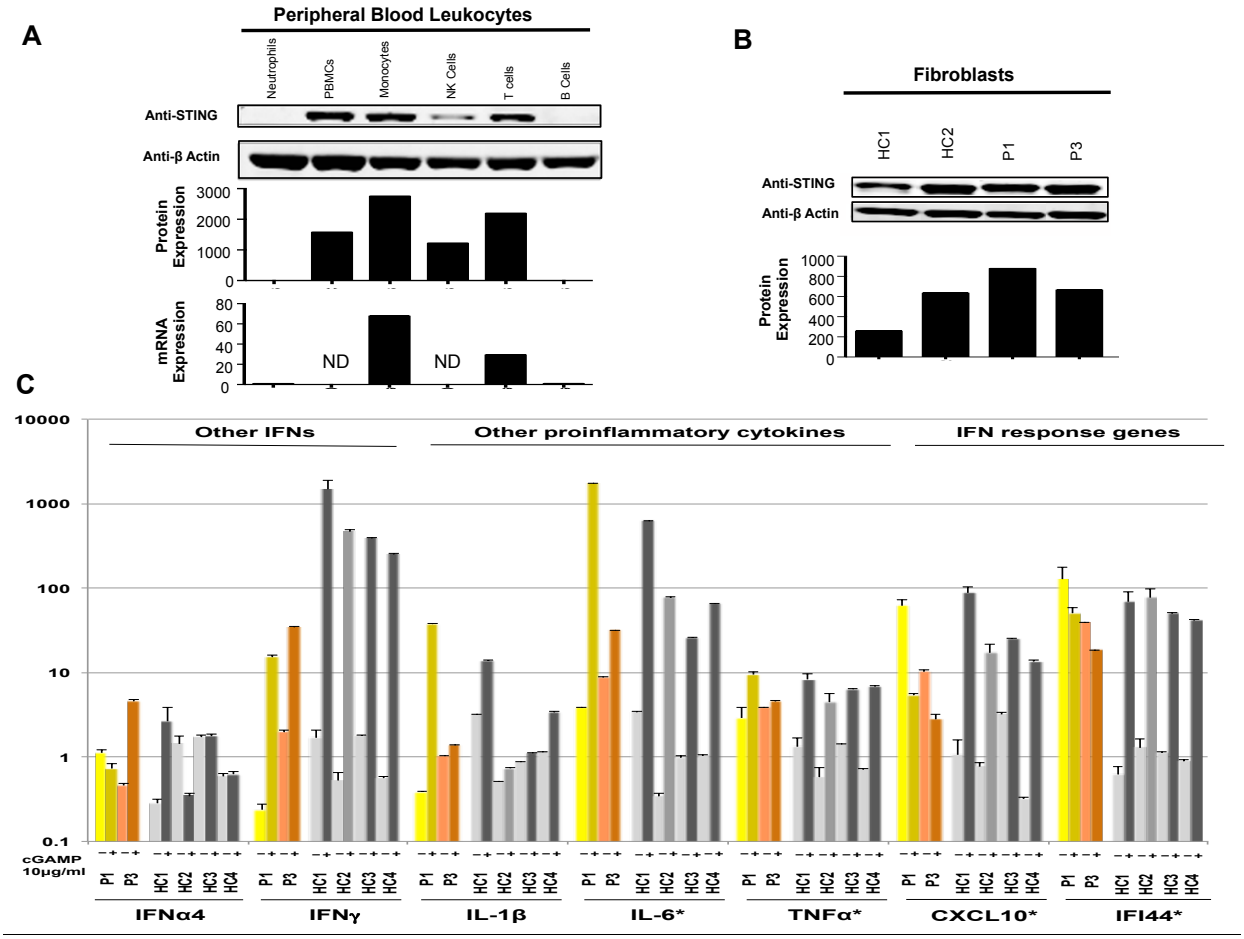

Panel A and B. STING mAb was used in a Western blot analysis to detect endogenous STING protein expression in neutrophils, PBMCs, sorted monocytes, NK cells, T and B cells from one healthy control (**Panel A**) and in fibroblasts from patients (Pt.1 and Pt.3) and two healthy controls (HC) (**Panel B**). The protein band was quantified and reported as arbitrary fluorescent units. The band intensities were normalized to β-Actin and the results are represented in the bar graph underneath. The lower bar graph in panel A shows qRT-PCR results of endogenous *TMEM173* message confirming that it is indeed absent in neutrophils and B cells. **Panel B** shows that healthy control and patient fibroblasts express STING protein. HC2=Pt.3's healthy sister. **Panel C**. qRT-PCR quantification of gene expression in cGAMP stimulated PBMCs, showing gene expression of the genes encoding interferons, IFNα4 (*IFNA4*) and IFNγ (*IFNG*), the proinflammatory cytokines, IL-1β (*IL1B*), IL-6 (*IL6*), TNFα (*TNF*), and two interferon response genes, *CXCL10* and *IFI44* in PBMCs from SAVI patients and controls stimulated or

not with 10 μg/ml cGAMP for 24 hours. The interferon response genes *CXCL10* and *IFI44*, and *TNF* are constitutively maximally upregulated in SAVI patients and could not be induced further in contrast to healthy controls, who had low constitutive activation and were readily inducible. In contrast to *IFNB1*, which is constitutively high in patients' PBMCs (Fig. 3C), *IFNA4* and *IFNG* expression in SAVI patients was similar to controls. *IL6* was constitutively higher expressed in SAVI patients than in controls but was further upregulated with cGAMP stimulation. *IFNA4* and *IL1B* were not consistently induced in either SAVI patients or controls. HC1=Pt.1's mother; HC2=Pt.1's father; HC3=Pt.3's mother; HC4=Pt.3's father. *For *IL6*, *TNF*, *CXCL10* and *IFI44*, statistically significant difference was observed between patients and controls for unstimulated samples. For stimulated samples, no statistically significant difference was observed between patients and controls.

Supplementary Figure S9. STAT phosphorylation is constitutively high in PBMCs from SAVI patients

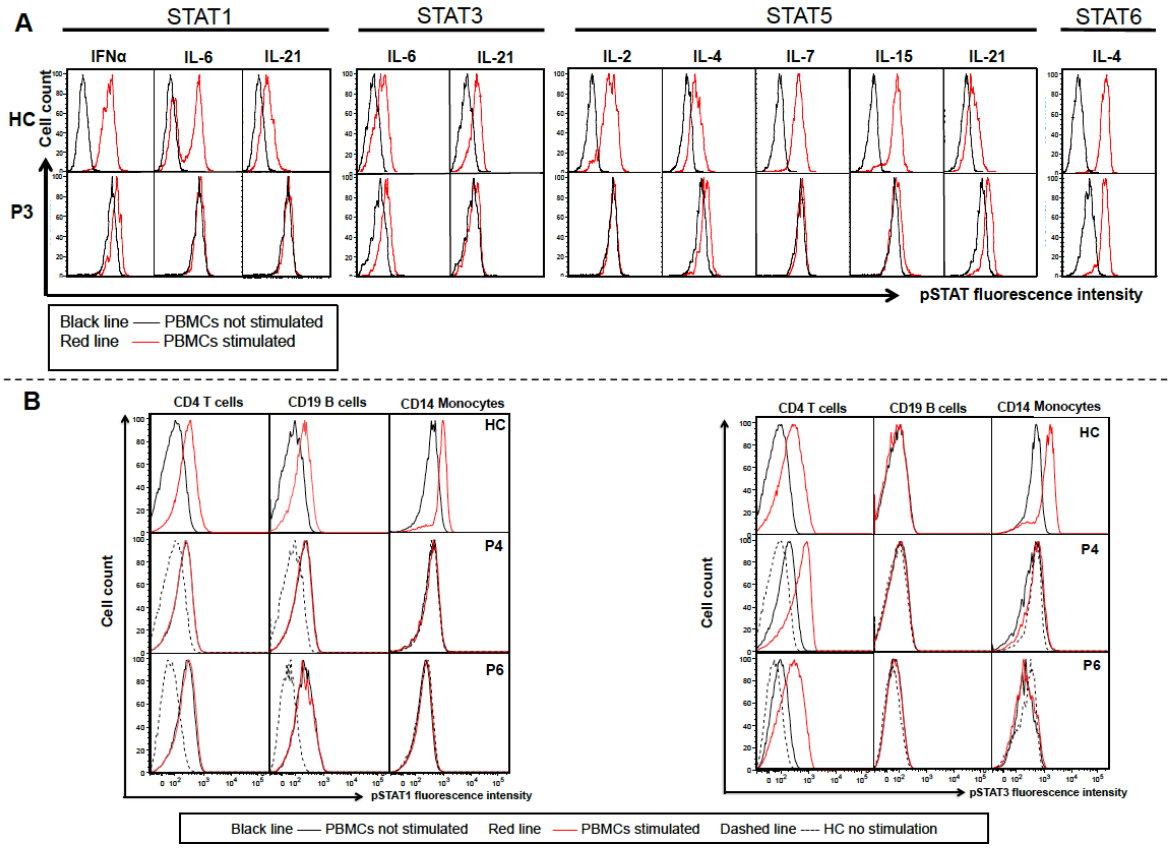

Panel A. PBMCs were stimulated with the agonist for 20 minutes and CD4+ T cells were assessed for pSTAT expression after 20 minutes of stimulation (Method 1). In contrast to cells from healthy control (HC), patient's cells (P3) were maximally phosphorylated before stimulation for STAT1, STAT3, STAT5 and, to a lesser extent, for STAT6 and were only slightly further upregulated after stimulation with IL-4, IL-6 and IL-21. **Panel B**. pSTAT1 or pSTAT3 analysis was performed (Method 2) for PBMCs from healthy control (HC) or patients (P4 and P6). Left: STAT1 phosphorylation was maximally upregulated in patient CD4+ T cells and could not be further induced through stimulation with IFNα. This was also observed in B cells. However, patient monocytes did not upregulate STAT1 phosphorylation either at baseline or after IFN stimulation in contrast to control monocytes. Right: patient CD4+ T cells expressed

increased pSTAT3 but, upon IL-6 stimulation, further induced pSTAT3 similarly to control. B cells did not respond in patients or control. Patient monocytes had no STAT3 phosphorylation at baseline and although IL-6 stimulation induced STAT3 phosphorylation in control monocytes, it did not do so in patient monocytes. The lack of response to stimulation in this assay likely reflects the fact that patient monocytes seem to undergo apoptosis *ex vivo*.

Supplementary Figure S10. Patient fibroblasts are constitutively active and are more sensitive to low levels of cGAMP stimulation than healthy control fibroblasts

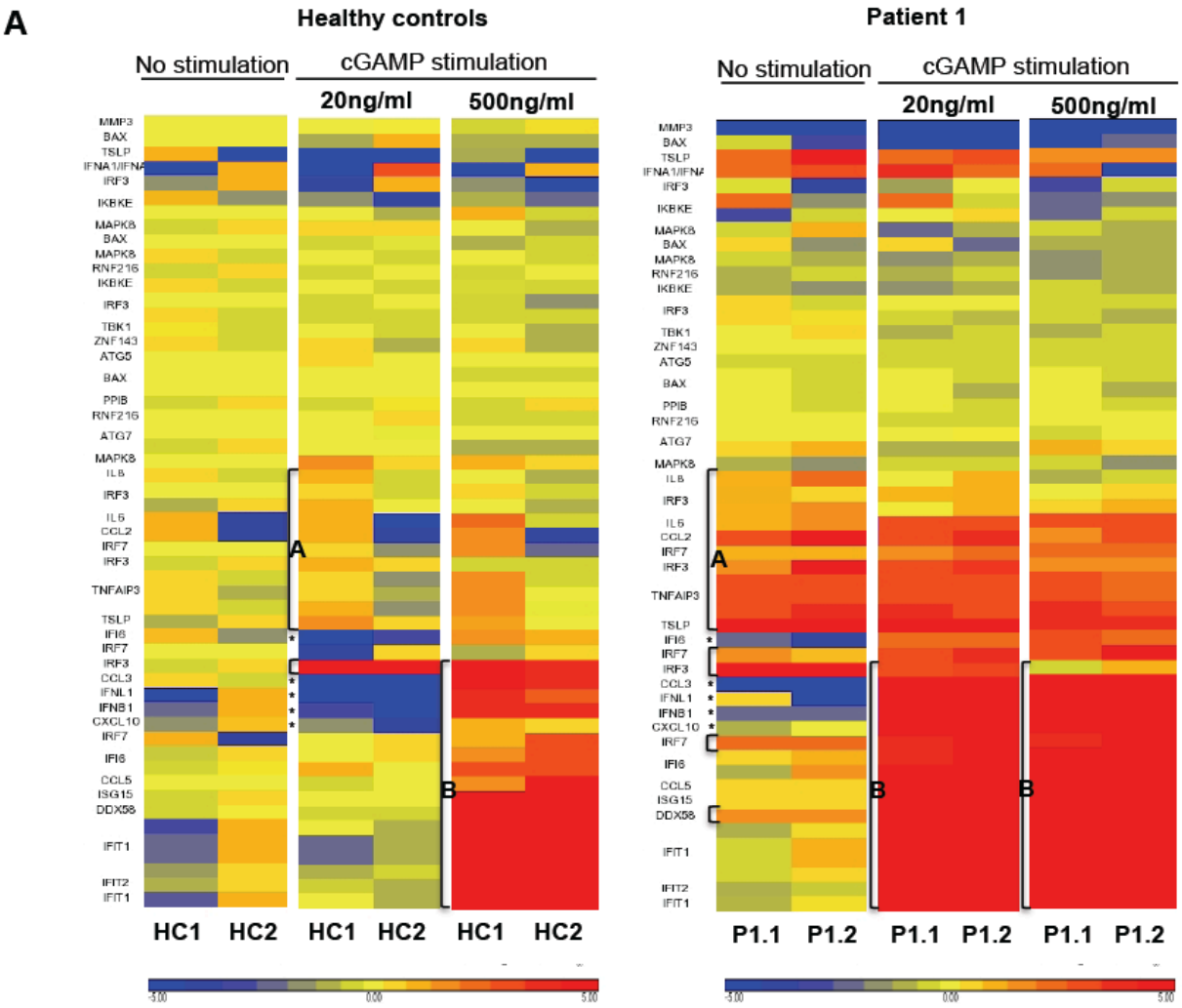

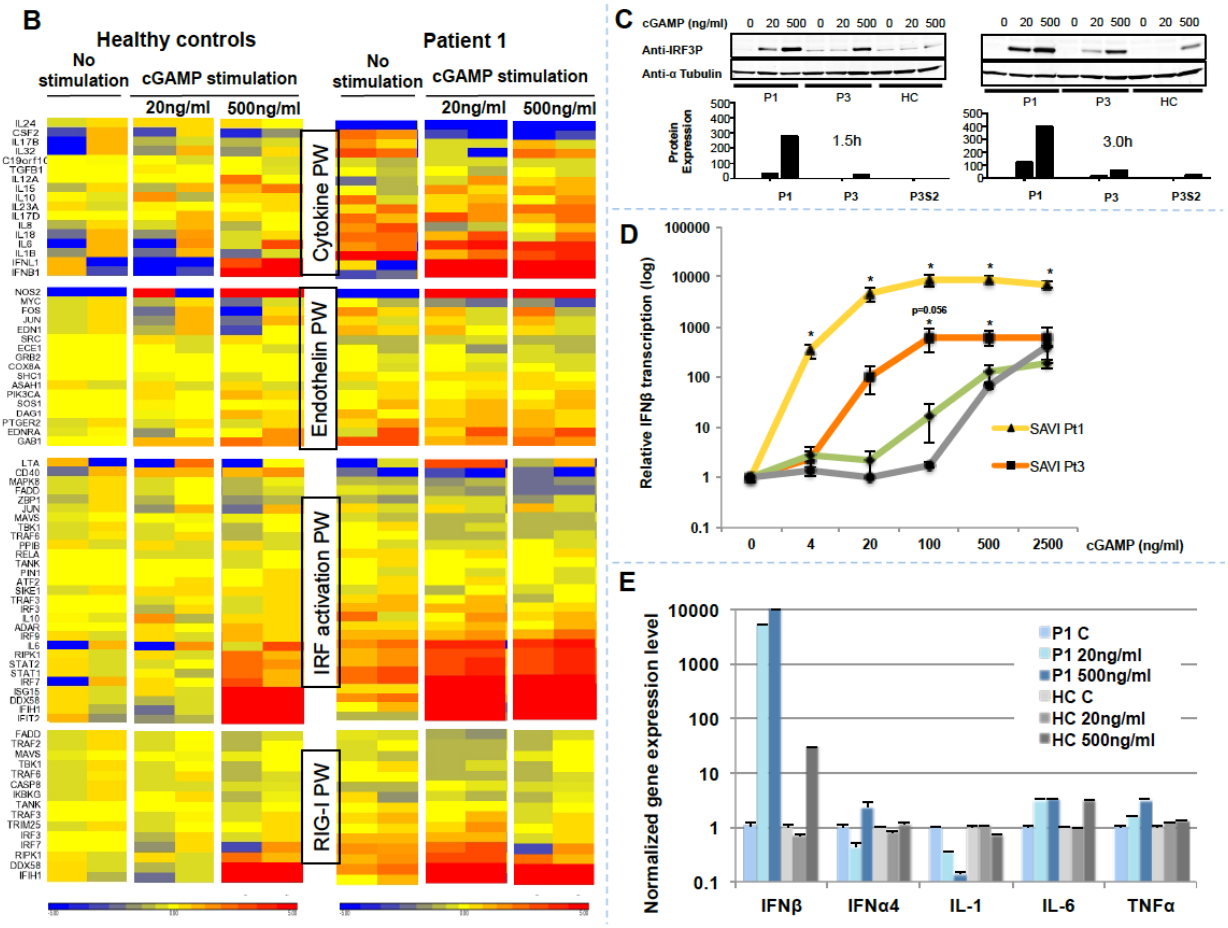

Panel A. A heat map shows expression of IRF3 regulated genes (Ingenuity Pathway analysis) in fibroblasts from a SAVI patient (Pt.1) and two healthy controls stimulated with 20 ng/ml and 500 ng/ml of cGAMP. Two different stimulation experiments were performed, denoted as P1.1 and P1.2. In red are upregulated genes and in blue are downregulated genes. Some genes in patient cells are constitutively upregulated, suggesting chronic activation. Gene set marked as A is upregulated in patient fibroblasts and only induced in HC1 after stimulation with 20 ng/ml of cGAMP. Gene set marked as B is maximally upregulated in the patient at 20 ng/ml of cGAMP stimulation but only with 500 ng/ml of cGAMP in both healthy controls. Asterisks indicate genes that are downregulated in unstimulated patient cells and with stimulation in the healthy controls. Bands without labels are isoforms of the above labeled gene transcript. **Panel B**. The gene expression profile is shown for markedly dysregulated canonical pathways identified by ingenuity pathway analysis (IPA), including cytokine pathway, endothelin pathway, IRF activation pathway and RIG-I pathway. Data indicate pathways constitutively activated in patient fibroblasts that get further upregulated with low concentrations of cGAMP stimulation in contrast to healthy controls, with only the higher concentration. **Panel C**. IRF3 phosphorylation (pIRF3) in cGAMP (20 and 500 ng/ml) stimulated patient and control fibroblasts were assessed after 1.5 and 3 hours stimulation, respectively with pIRF3 mAb by Western blot. Protein expression is reported as arbitrary fluorescent units and band intensities were normalized to α-tubulin, as depicted in the lower portion of the figure. Patient fibroblasts had markedly increased pIRF3 at both 1.5 and 3 hours after stimulation. Pt.1 had even stronger expression of pIRF3 than Pt.3, consistent with the higher IFNβ encoding gene (*IFNB1*) transcription after stimulation in Pt.1. **Panel D**. qRT-PCR quantification of *IFNB1* message is performed after

cGAMP stimulation for 4 hours in haplotype-matched fibroblasts from 2 SAVI patients, 3 CANDLE disease controls and 4 healthy controls. Shown is the fold change of *IFNB1* message after stimulation over the mean of non-stimulated conditions. For patients, each point in the graph is the result of the average of 3 separate experiments. Healthy controls and CANDLE controls were combined from the 2 patients' experiments and averages were plotted. Error bars indicate SEM. Asterisks indicate $p<0.05$ comparing each patient's experiment to controls. **Panel E**. qRT-PCR gene expression analysis in cGAMP stimulated fibroblasts from Pt.1 and healthy controls (HC) (n=4) showed *IFNB1* was more strongly induced in Pt.1 than in HC. *IFNA4* was not induced in HC, only minimally in Pt.1. *IL1B* was more suppressed in Pt.1 than in HC. *IL6* and *TNF* were minimally induced in both Pt.1 and HC.

Supplementary Figure S11. Transfection of mutated *TMEM173* in HEK293T cells activates the gene encoding IFNβ (*IFNB1*) promoter activity in a dose dependent manner

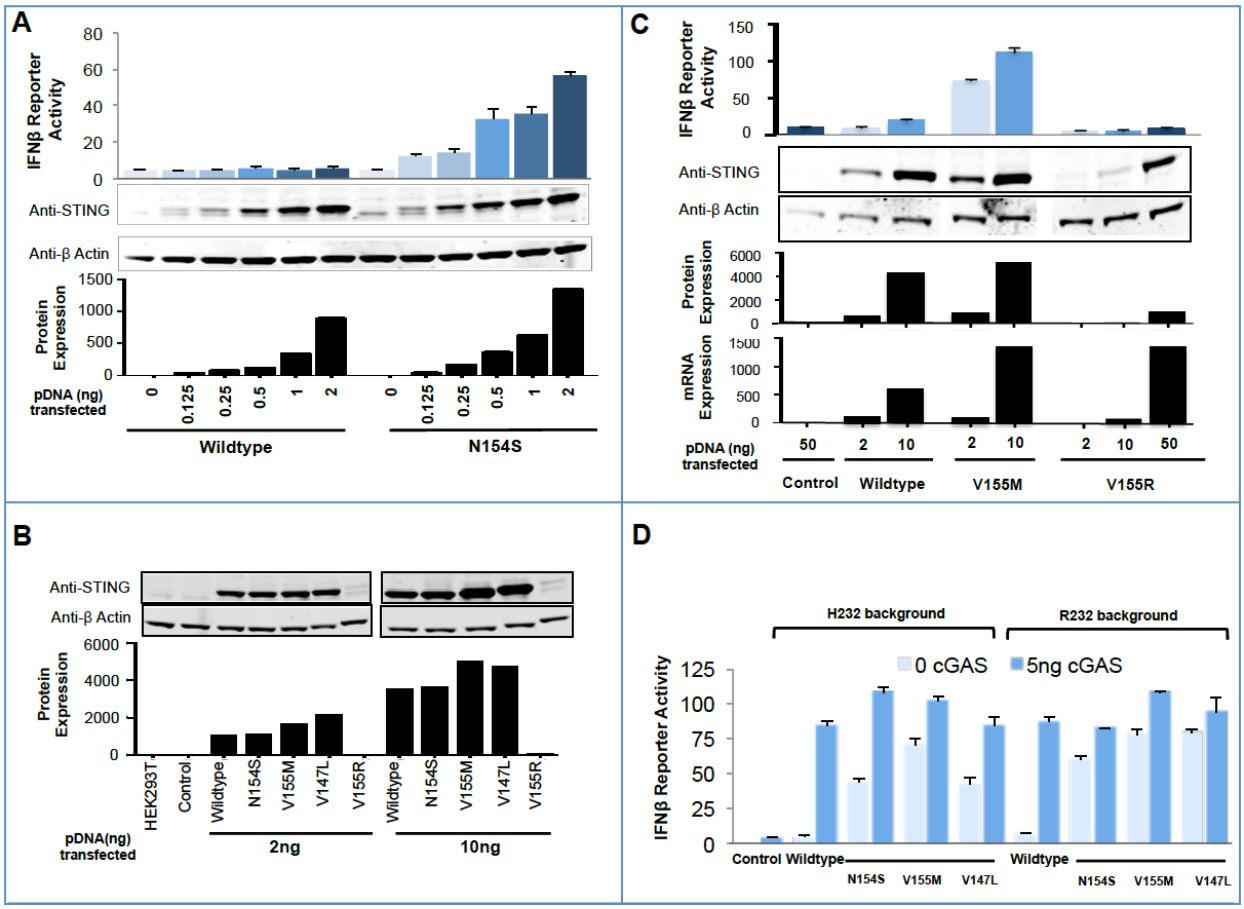

STING mutant constructs on the most common haplotype background (R232) were used in transfection assays unless otherwise indicated. Western blots were performed on the lysate of the *TMEM173* transfected cells and the expressed STING protein was quantified and reported as arbitrary fluorescent units. The band intensities were normalized to β-Actin and the results are represented in the bar graph underneath. **Panel A**. Different dose wildtype and N154S mutant STING constructs were co-transfected into HEK293T cells with an IFNβ encoding gene (*IFNB1*) promoter reporter construct and a control Renilla luciferase construct. *IFNB1* reporter activity was measured using a luciferase assay. The control group was not transfected with the *TMEM173* DNA constructs. *IFNB1*promoter activity was not induced in cells transfected with wildtype *TMEM173* at the pDNA concentrations transfected, but it was induced in a dose dependent manner in cells transfected with the N154S construct at protein expression levels similar to wildtype. **Panel B**. 2 ng and 10 ng of wildtype and mutant (N154S, V155M, V1476L and V155R) pDNA were transfected and the control group consisted of pMAXGFP. Protein expressed from the constructs with the putative disease mutations and wildtype protein are similarly expressed. However, the construct carrying the loss of function mutation, V155R is not expressed. **Panel C**. STING constructs with the SAVI disease associated mutation, V155M and the loss of function mutation, V155R, and wildtype were transfected into HEK293T cells at different doses in an attempt to achieve equivalent protein expression. *TMEM173* mRNA expression was assessed in addition to *IFNB1* reporter activity, and protein expression levels. Only *TMEM173* constructs with the disease associated mutation, V155M caused *IFNB1* promoter transcription. With the loss of function V155R mutant, 50 ng of transfected pDNA led to mRNA levels equivalent to 10 ng of wildtype or the V155M mutant, but the protein

expression is only comparable to 2 ng of wildtype and the V155M mutant. No reporter activity is seen for the loss of function mutant. The control group consisted of pMAXGFP. **Panel D**. A less common haplotype carrying a histidine (H) at position 232 is reported to have reduced binding affinity to the cGAMP ligand we used in our assays. We thus tested the STING constructs on the H232 background with co-transfection of cGAS, the endogenous enzyme that leads to the production of the endogenous high affinity cGAMP. Our data show that the three disease causing mutant constructs have constitutively higher *IFNB1* promoter activity on either the R232 and on the H232 background and can be further upregulated with transfection of cGAS, confirming that the disease causing mutations induce higher *IFNB1* transcription regardless of the *TMEM173* background. The control consisted of pDNA expressing cGAS.

Ref: Yi G, Brendel VP, Shu C, Li P, Palanathan S, Cheng Kao C. Single Nucleotide Polymorphisms of Human STING Can Affect Innate Immune Response to Cyclic Dinucleotides. *PLoS One* 2013;8:e77846.

Supplementary Figure S12. STING expression in endothelial cells, in bronchial endothelium and in alveolar Type 2 pneumocytes

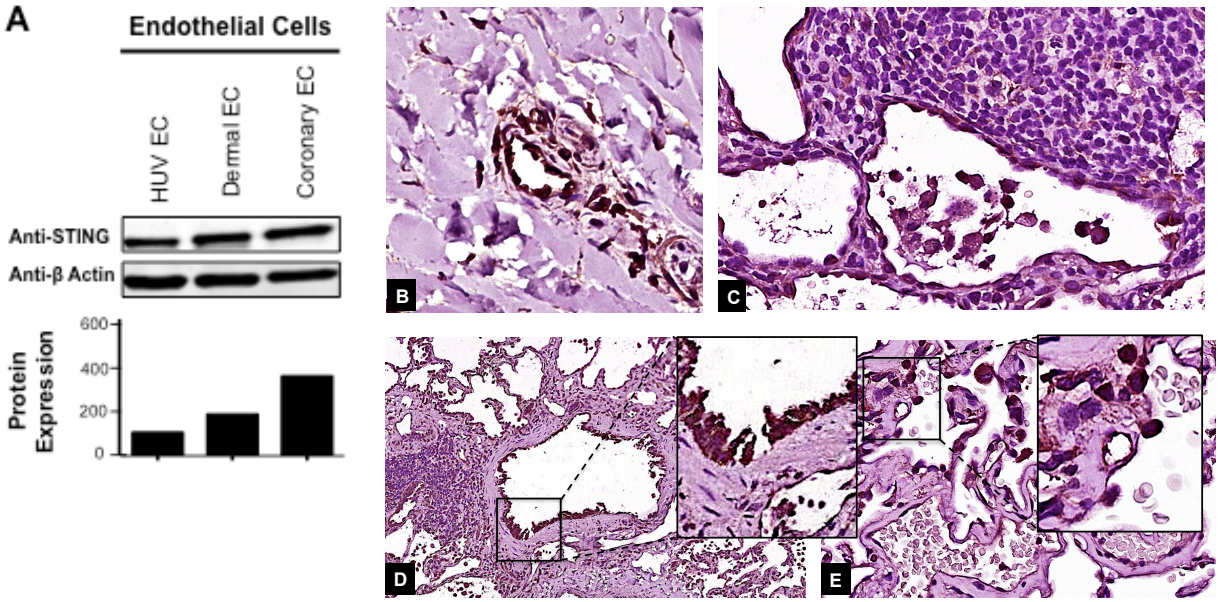

Panel A. Western blot of cell lysates from commercially available endothelial cells blotted with anti- STING and anti- β-Actin antibodies show expression of STING in endothelial cells. The protein bands were quantified and reported as arbitrary fluorescent units and band intensities were normalized to β-Actin. **Panel B**. STING staining of an unaffected skin vessel from a healthy control shows STING staining of the endothelial cell as well as nuclei of surrounding cells, which have the shape of pericytes. **Panel C**. Lung biopsy from affected patients showed positive staining for STING protein in alveolar macrophages and alveolar lining cells (Type 2 pneumocytes). (Original magnifications 400x) **Panels D and E**. Healthy control lung tissue showed strong and diffuse staining of STING protein in bronchial epithelium (**Panel D**) and Type 2 pneumocytes (**Panel E**). (B. Original magnification 100x; C. Original magnification 200x).

Supplementary Figure S13. Endothelial cell activation in patients' skin biopsies and in primary HUVECS stimulated with cGAMP

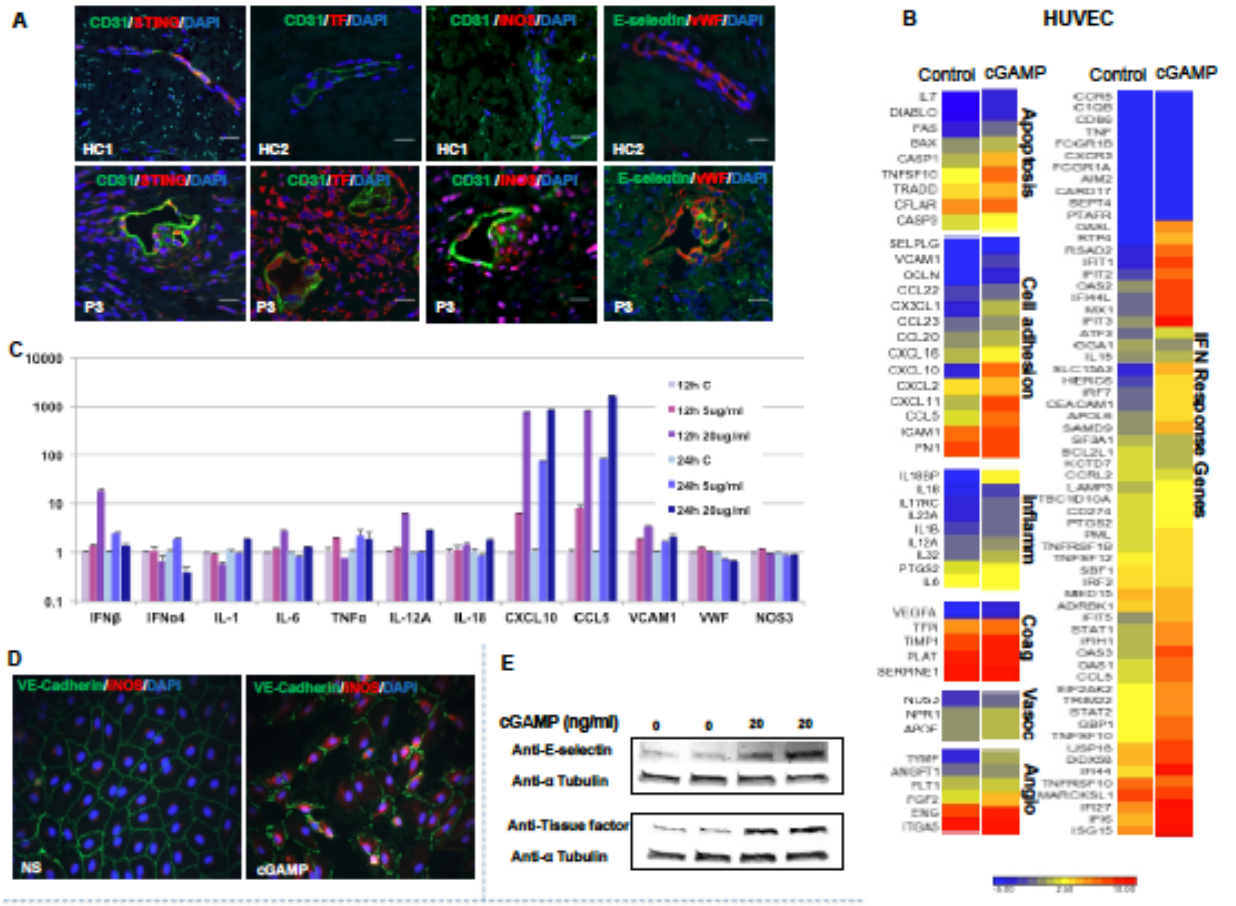

Panel A shows tissue repeat immunofluoresence staining in a skin biopsy from Pt.3 and healthy donor controls (HC1 and HC2). Endothelial cell marker CD31 (green) was co-stained with STING (red), coagulation marker Tissue Factor (TF, red), and inflammatory marker iNOS (red). Endothelial cell activation marker E-selectin (green) was co-stained with von Willebrand factor (vWF). Shown is a damaged endothelial cell layer in patients (lower panels) and a preserved endothelial cell layer in healthy donor controls (upper panels); TF and iNOS are upregulated in patients endothelial cells while STING expression shows the similar pattern in both control and Pt.3 endothelial cells. Expressing of E-selectin in endothelial cells indicates endothelial cell activation. Nuclei are stained blue with DAPI. (Scale bar: 20 μm). **Panel B** shows gene expression in human umbilical vein endothelial cells (HUVEC) without and with cGAMP (20 μg/ml) stimulation. Depicted are heat maps of pathway genes for apoptosis, cell adhesion, inflammation, coagulation, vasoconstriction, angiogenesis and IFN response genes. In response to cGAMP stimulation endothelial cells increase transcription of key genes in each of these pathways. Red indicates higher expression value and blue lower expression value. **Panel C**. Expression of key genes in each pathway found to be upregulated in the gene expression analysis in HUVECs activated by cGAMP shown in Panel B were validated by qRT-PCR**.** After 12h or 24h of cGAMP stimulation, the genes encoding IFNβ (*IFNB1*), CXCL10 (*CXCL10*), CCL5 (*CCL5*), VCAM1 (*VCAM1*), IL-18 (*IL18*), IL-6 (*IL6*), TNFα (*TNF*), and IL-12A (*IL12A*) are upregulated to different extents. The genes encoding vWF (*VWF*), NOS3 (eNOS; *NOS3*), IFNα (*IFNA*) and IL-1 (*IL1B*) are not changed. **Panel D**. Primary dermal microvascular endothelial cells (HMVEC) were seeded into a 12 well plate at 80,000 cells/well and cultured

until confluent. Cells were treated with or without 20µg/ml cGAMP for 24 hours and fixed with 4% paraformaldehyde. Cells were stained with endothelial marker VE-Cadherin (green) and inflammatory marker iNOS (red). After cGAMP treatment endothelial cells damage is seen, and cells lost cell-cell contact causing disruption of the monolayer. Damaged endothelial cells are iNOS positive. NS: no stimulation. Magnification: 40X. **Panel E**. Shown are immunoblots of biological duplicates of human dermal endothelial cells treated with vehicle, or 20 µg/mL of cGAMP for 24hrs. Blots were probed with antibodies specific to E-selectin, Tissue Factor, and tubulin and depict dose dependent upregulation with cGAMP stimulation.

Supplementary Figure S14. Cell apoptosis and lack of monocyte differentiation in patients with SAVI

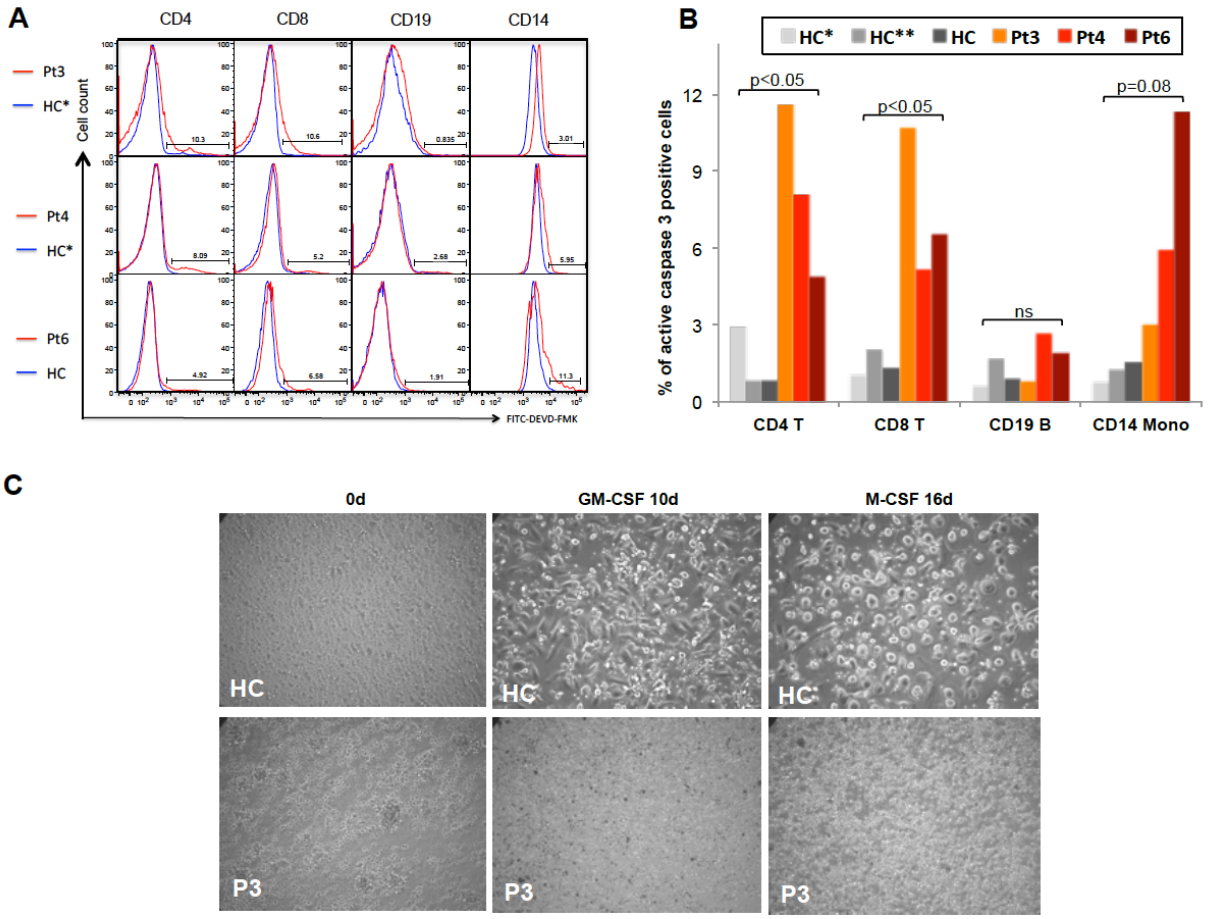

Panel A shows flow cytometry analysis of active caspase 3 expression in the indicated PBMC cell populations from Pt.3, Pt.4 and Pt.6, each with a healthy control (HC). Gated are active caspase 3 positive cells and numbers are percentages of positive cells in patients. **Panel B** graphed the percentage of active caspase 3 positive cells depicted in Panel A. **Panel C**. Primary human monocytes isolated from healthy control (HC) and SAVI patients were seeded at 150,000 cells/cm^2. Cells were differentiated into macrophages using 20 ng/ml human Granulocyte-macrophage colony-stimulating factor (GM-CSF) or 50 ng/ml human macrophage colony-stimulating factor (hM-CSF) for 10-16 days. Control monocytes attached and exhibited macrophage-like morphology after GM-CSF or M-CSF treatment. The patient's cells did not

differentiate into macrophages under both conditions. At the end of the culture period most cells had died in culture.

Supplementary Figure S15. JAK kinase inhibitor (tofacitinib) can inhibit STAT1 and STAT3 phosphorylation in SAVI patients

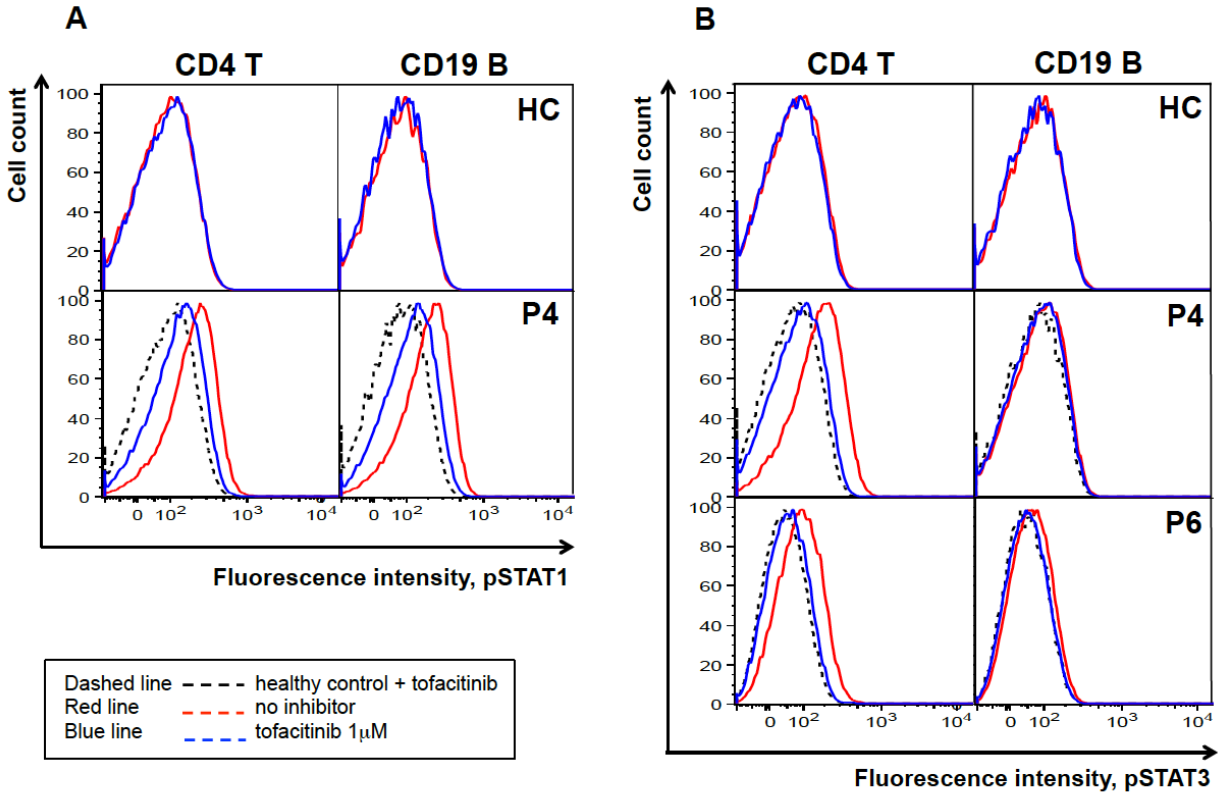

PBMCs from SAVI patients and healthy controls (HC) were treated or not with 1 μM of tofacitinib for 4 hours. STAT1 or STAT3 phosphorylation in CD4 T and CD19 B cells was analyzed by intracellular staining of pSTAT1 and pSTAT3 in addition to cell surface marker staining. **Panel A**. pSTAT1 was not downregulated by tofacitinib in cells from healthy control (HC, upper graph), suggesting that pSTAT1 is not upregulated in healthy controls. In contrast, STAT1 was constitutively phosphorylated in Patient 4's cells compared with HC's cells, and was downregulated by tofacitinib (lower graph). **Panel B**. Similarly to pSTAT1, pSTAT3 was also not downregulated by tofacitinib in cells from healthy control (HC, upper graph). pSTAT3 was constitutively expressed only in CD4 cells but not in CD19 B cells from Patients 4 (P4) and 6 (P6) (middle and lower graphs). In both patients, pSTAT3 on CD4 cells was downregulated by tofacitinib to the level of healthy controls.

Supplementary Figure S16. JAK kinase inhibitor (tofacitinib) can inhibit cGAMP induced transcription of interferon-β encoding gene (*IFNB1*) and interferon regulated genes

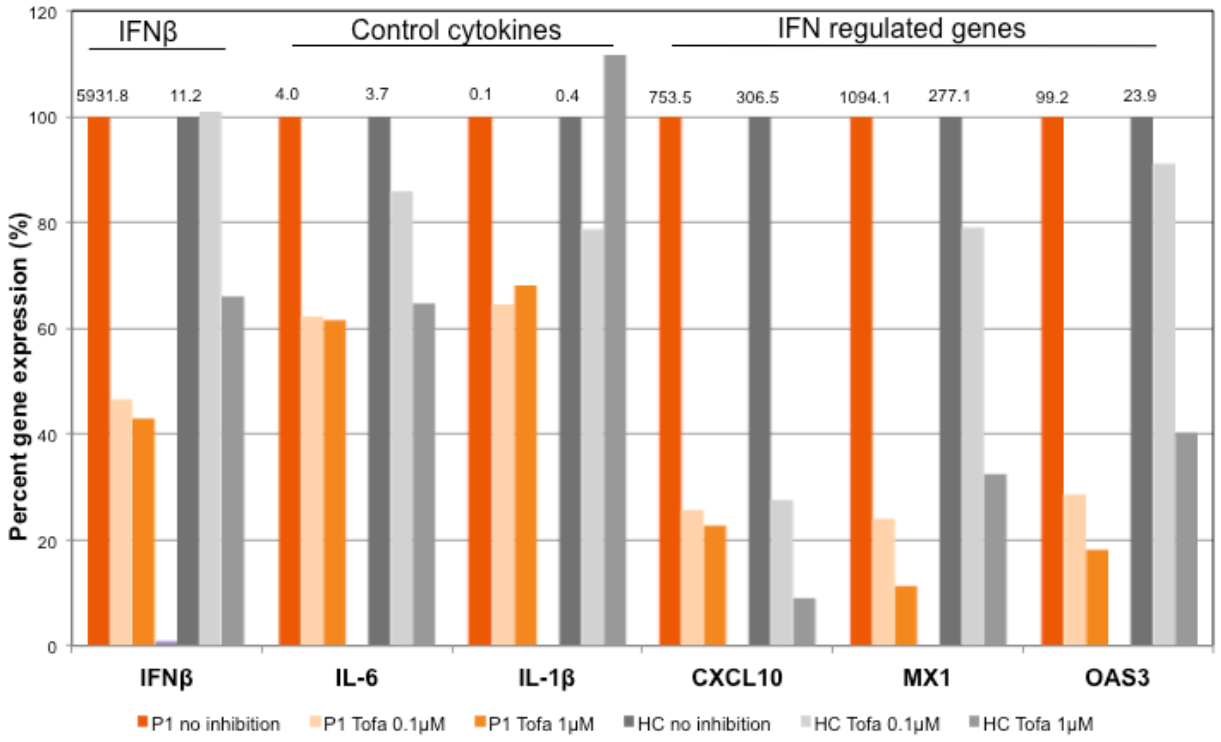

qRT-PCR analysis of gene expression in fibroblasts from Pt.1 and a healthy control stimulated with 500 ng/ml cGAMP, in the presence or not of tofacitinib (0.1 or 1 μM) is shown. Gene expression level after cGAMP stimulation without tofacitinib was set as 100%, and the percentage of the residual expression is graphed for the tofacitinib inhibition experiments. Expression of IFN regulated genes (*CXCL10*, *MX1* and *OAS3*) was suppressed, especially at the 1 μM concentration of tofacitinib. The other genes are either not or only minimally suppressed. The numbers on top of the bar denotes the fold induction of the reaction over unstimulated.

Supplementary Figure S17. Hematologic findings, acute phase reactants and B cell subsets in patients with SAVI

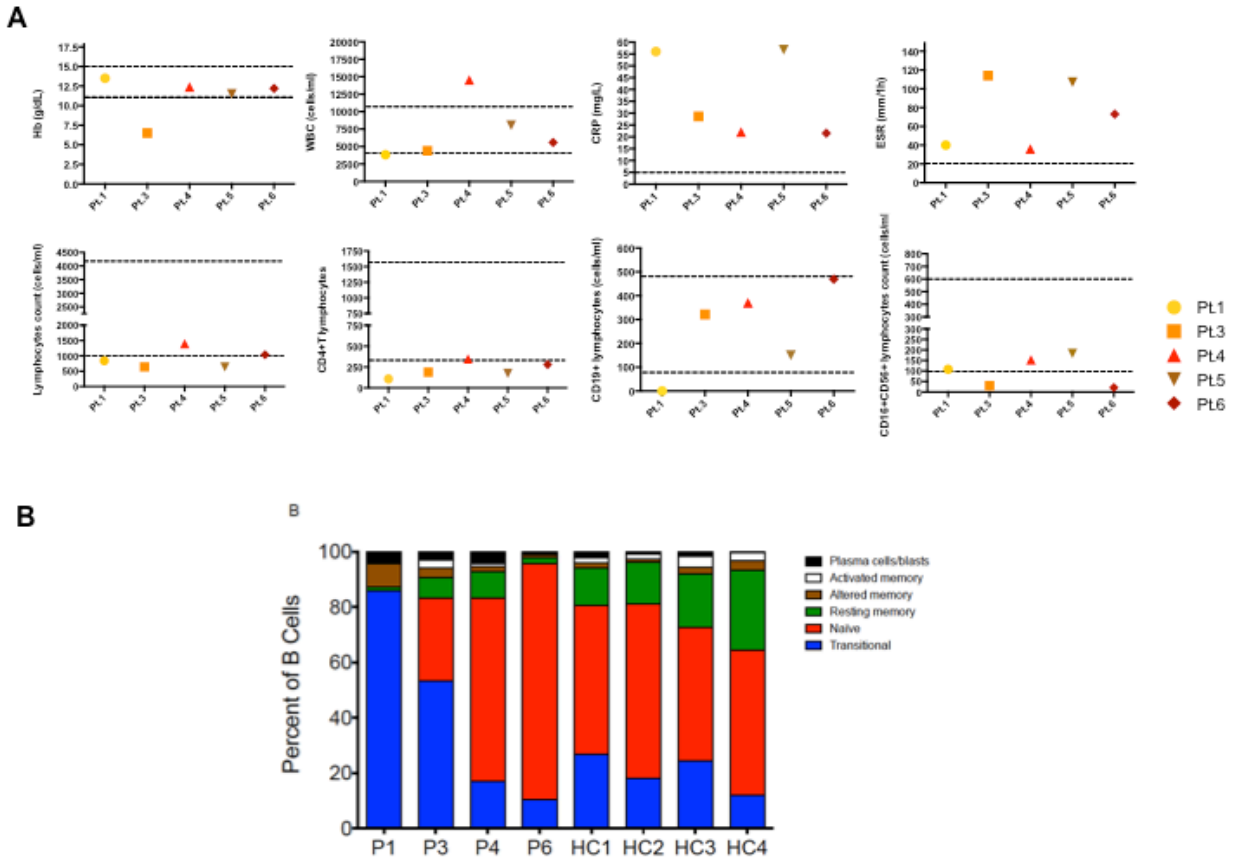

Panel A shows plotted values of the blood levels of hemoglobin (Hb), white blood cells (WBC), the acute phase reactants: C-reactive protein (CRP) and erythrocyte sedimentation rate (ESR), total lymphocytes, CD4+ T lymphocytes, CD19+ (B) lymphocytes and CD16+CD56+ (NK) lymphocytes in Pt.1, Pt.3, Pt.4, Pt.5 and Pt.6. The plotted values represent the laboratory results at the last clinical visit. The dashed lines represent the lower and upper limit of normal values. **Panel B** depicts the B cell subsets by peripheral blood flow cytometry in 4 patients with SAVI and 4 healthy controls. The patients present with a lower percentage of resting B cells. Pt.1 is on rituximab treatment, which causes B cell depletion.

III. Supplementary Tables

Supplementary Table S1: Clinical characteristics of SAVI

	PATIENT 1	PATIENT 2	PATIENT 3	PATIENT 4	PATIENT 5	PATIENT 6
DEMOGRAPHICS						
Current Age yr	7	Deceased age 15	16	9	Deceased age 14	23
Sex	Female	Male	Female	Male	Female	Male
Ethnicity/Origin	French-Canadian	American/ Caucasian	Turkish	Hispanic	American/ Caucasian	American/ Caucasian
Age of clinical presentation	Neonatal	8 weeks	6 weeks	1 week	Neonatal	3 days
Symptoms of initial presentation	Tachypnea in perinatal period, erythematous - purpuric plaques on tip of nose and cheeks since age 4mo	Telangiectatic erythema and scaling on cheeks and ears	Fever and pustular rash	Fever, ulcers on toes and fingers, generalized rash and pustules on face	Tachypnea in perinatal period, pustular lesions on the heels and toes since age 6mo	Fingers swelling
FEATURES OF SYSTEMIC INFLAMMATION						
Elevated acute phase reactants*/ Fever/ Chronic anemia	Yes / Yes / Yes	Yes / Yes / Yes	Yes / Yes / Yes	Yes / Yes / Yes	Yes / Yes / Yes	Yes / No / Yes
CLINICAL FEATURES OF VASCULITIS						
Acral violaceous plaques and nodules on the face, nose and ear lobes	Yes	Yes	Yes	Yes	Yes	Yes
Painful distal ulcerative lesions with purulent discharge or tissue infarcts	Yes	Yes	Yes	Yes	Yes	Yes
Oral ulcers, pustules or vesicles	Yes	ND	Yes	Yes	Yes	Yes / Soft palate and posterior pharyngeal wall
Generalized pustules	Yes	Yes	Yes	Yes	Yes (acropustulosis)	Yes
Eschars	Yes / Eschar overlying deep necrotic ulcer of the left cheek	Yes / Violaceous crusted plaques and nodular lesions with superficial ulceration	Yes	Yes / Distal extremities	Yes / Plantar area	Yes / Forelegs
CLINICAL FEATURES OF VASCULAR/TISSUE DAMAGE						
Livedo reticularis (localized to extremities and transient during cold exposure)	Yes	Yes	Yes	Yes	Yes	Yes
Raynaud phenomenon	Yes	ND	Yes	ND	Yes	Yes
Telangiectasia	Yes	Yes	Yes	Yes	Yes	Yes
Nailfold capillary tortuosity and/or periungual erythema	Yes / Prominent violaceous periungueal erythema	Yes / 2+ tortuosity and 2+ capillary loop loss	ND	ND	ND	Yes
Gingival capillary dilatation	ND	ND	Yes	ND	ND	ND
Nail dystrophy or loss	Yes / Clubbing	Yes / Dystrophy of finger and toenails	Yes / Dystrophy	Yes / Dystrophy	Yes / Dystrophy	Yes / Dystrophy and loss
Amputation of extremities/onset	No	No	Yes / 3yr	Yes / 18mo	Yes / 8yr	Yes / 11yr (noticed to have shortened digits, sclerosis and acral osteolysis)
Nasal septum perforation	No	No	Yes	Yes	Yes	Yes

	PATIENT 1	PATIENT 2	PATIENT 3	PATIENT 4	PATIENT 5	PATIENT 6
PULMONARY MANIFESTATIONS						
Interstitial lung disease on CT	Yes / Chest CT with diffuse interstitial edema (8mo); lung biopsy: interstitial chronic inflammation, multifocal lymphoid formations, alveolar hyperplasia and mild pulmonary fibrosis. Paratracheal adenopathy	Yes / PFT with moderate-severe restrictive defect Paratracheal adenopathy	Yes / Mild interstitial lung disease PFT with mild restrictive defect Hilar adenopathy	No / Recurrent wheezing episodes Mild mediastinal adenopathy	Yes / Bilateral lung infiltrates, patchy interstitial lung disease, Prominent hilar lymphadenopathy	Yes / Pneumonias from 2-4 yrs and from 12-14 yrs; mild interstitial lung disease PFT with mild restrictive defect Paratracheal adenopathy
Lung fibrosis	Yes	Yes	No	No	Yes	No
MUSCULOSKELETAL MANIFESTATIONS						
Myositis	ND	Yes	No	No	Yes	No
Arthritis/arthralgia	No / Arthralgia with strenuous exercise	No / Yes	No / No	No / No	Erosive RF+ Rheumatoid Arthritis	No / No
Chronic deforming arthritis	No	No	No	No	Yes	No
Joint stiffness	No	Yes	No	No	Yes	No
HEMATOLOGIC AND IMMUNE-RELATED ABNORMALITIES						
IgG mg/dL (normal range for age)	**2130** (504-1465)	ND	**5150** (549-1584)	**1630** (572-1474)	**2750** (642-1730)	**2560** (642-1730)
IgA mg/dL (normal range for age)	**375** (27-195)	ND	**485** (61-348)	**590** (34-305)	**588** (91-499)	**534** (91-499)
IgM mg/dL (normal range for age)	122 (24-210)	ND	85 (23-259)	82 (32-208)	303 (34-342)	51 (34-342)
C3, C4 levels	Normal	Normal	Normal	Normal	Normal	Normal
Autoantibodies* **	***ANA*: pos** *ENA*: pos (anti-Ro) x1 *ACA IgM*: pos x1, now neg *anti-β2GP1*: pos x1, now borderline pos	Anti-phospholipid antibody pos x1	***ANA*: pos** *LAC*: neg until age 3yo, now weak pos *ACA IgG*: neg until 18 mo, now pos (low titer)	Autoantibodies testing negative on 3-4 occasions	*ACA IgG*: pos x1 ***RF, anti-CCP*:** high pos *c-ANCA*: pos x1, now neg x5	***ANA*: pos** *ACA IgG*: pos x1, now neg x2 *anti-RNP*: pos 2x, now neg. X3 *LAC*: neg x1 (17yo), now weak pos x3 *c-ANCA*: weak pos x1, now neg x2
Leukopenia	Yes	Yes	Yes	Yes (fluctuating levels)	No	Yes
Lymphopenia with normal B cell count	Yes (Low B cell count on rituximab)	ND	Yes	Yes	Yes	Yes
Thrombocytosis	Yes	ND	Yes	Yes	Yes	No
Recurrent infections	Recurrent URTIs, pneumonia (1x)	Pneumonias, recurrent secondary skin infections, cellulitis	Recurrent otitis externa, ear colonization by Pseudomonas aeruginosa, secondary skin infections, cellulitis	Pansinusitis, secondary skin infections, cellulitis	Recurrent oral candidiasis, URTIs, sinusitis, pneumonia (2x), bronchia and sinus colonization by Pseudomonas aeruginosa	Recurrent pneumonias, secondary skin infections, skin colonization by Pseudomonas aeruginosa and Staphylococcus aureus

	PATIENT 1	PATIENT 2	PATIENT 3	PATIENT 4	PATIENT 5	PATIENT 6
OTHER CLINICAL ABNORMALITIES						
Birth weight (Kg) / Birth length (cm)	2.99 (AGA) / 48.5	3.83 (AGA) / ND	4 (LGA) / 54	3.75 (AGA) / 51	2.97 (AGA) / ND	3.53 (AGA) / 53.3
Weight < 3rd Percentile / Height < 3rd Percentile	Yes (recovered) / Yes (3rd – 5th Percentile)	Yes / Yes	Yes / Yes	Yes (3rd – 5th Percentile) / Yes	Yes / Yes	Yes (recovered) / Yes (recovered to 5th – 10th Percentile)
Association of symptoms with cold exposure	Yes	Yes	Yes	Yes	Yes	Yes
Arterial hypertension	Yes	ND	No	Yes	No	No
Cognitive function	Normal	Normal	Normal	Normal	Normal	Normal
FAILED TREATMENTS						
Steroids	Methylprednisolone pulses, prednisone	Methylprednisolone pulses, prednisone	Prednisone	Prednisone	Prednisone	Prednisone
DMARDs	Hydroxychloroquine, mycophenolate mofetil, cyclophosphamide	Hydroxychloroquine, colchicine, methotrexate, azathioprine	Methotrexate, cyclophosphamide	Colchicine, thalidomide, cyclosporine	Hydroxychloroquine, methotrexate	Hydroxychloroquine, leflunomide, azathioprine,
Biologics	IVIG, infliximab, belimumab, rituximab (since 2009)	No	Etanercept, anakinra, tocilizumab	IVIG, infliximab	IVIG	Etanercept
Other	Aspirin, nifedipine, amlodipine, hydrochlorothiazide, pamidronate, calcium carbonate, vitamin D, iron, valacyclovir, itraconazol, salbutamol	Nifedipine	Clotrimoxazol	Heparin, aspirin, nifedipine, morphine, amitriptyline	Naproxen, aspirin, nifedipine, calcium carbonate, iron, folic acid, alendronate, fluticasone, albuterol	Aspirin, nifedipine, amlodipine, folic acid, cefixime, acyclovir, nistatin, nabumetone, gabapentin, methadone, oxycodone, amitriptyline
MUTATION / INHERITANCE	N154S / AD - *de novo*	V155M / AD - *de novo*	N154S / AD - *de novo*	V147L / AD - *de novo*	N154S / AD**	N154S / AD**

* Acute phase reactants denote C-reactive protein (CRP) and erythrocyte sedimentation rate (ESR)

** Fathers were not available for confirmation of *de novo* inheritance; ND denotes not described; AD denotes autosomal dominant; CT, computed tomography; ANA, antinuclear antibody; ACA, anticardiolipin antibody; anti- β2GP1, anti- beta2 glycoprotein 1 antibody; RF, rheumatoid factor; anti-CCP, anti-cyclic citrullinated peptide antibody; cANCA, cytoplasmic antineutrophil cytoplasmic antibody; anti-RNP, anti-ribonucleoprotein antibody; anti-PR3, anti-proteinase 3 antibody; URTI, upper respiratory tract infection; AGA, appropriate for gestational age; LGA, large for gestational age; IVIG, intravenous immunoglobulin; AD, autosomal dominant

*** Antibodies in bold were persistently positive

Description of the autoantibodies titers over time:

Five out of six patients had comprehensive autoantibody evaluation over time. ANA is positive in 3/5 patients and remained positive over time. Among the ENA antibodies, 3/5 patients were positive; anti-Ro (anti-SSA) antibodies were seen in one patient, and anti-RNP antibodies in 2 other patients. The anti–RNP antibodies became negative in both patients over time. Anti-dsDNA was negative in all patients.

Antibodies associated with antiphospholipid syndrome (APS), including ACA, LAC and anti- β2 GP1, were serially tested in 5 patients. 3/5 patients had low titer ACA IgG, with the highest titer observed in one patient being 52 GPL. One of these patients became negative over time, and titers in the other 2 were below 30 GPL on consecutive tests. ACA IgM was only positive in 1/5 patients with an initial titer of 41 MPL and then titers became negative over time. In comparison, titers in anti-phospholipid syndrome (APS) typically rise to levels above 80 GPL for ACA IgG and ACA IgM. LAC was only positive in 2/5 patients who were negative in infancy and became positive at the ages of 16yrs and 23yrs, respectively. Anti-β2GP1 antibody was transiently positive in only one patient who is now borderline positive.

C- and p-ANCA antibodies were also evaluated in the 5 patients. Two patients had transiently low titer c-ANCA positivity that became negative over time. Patient 3 was transiently only weakly positive at the age of 3 and was at that time diagnosed with c-ANCA positive vasculitis until her titers became negative. P-ANCA was only positive in Patient 3 at the same age she was found to be c-ANCA positive, p-ANCA titers were negative on a repeat evaluation.

Supplementary Table S2: Hematologic findings and acute phase reactants in 5 patients with SAVI

	PATIENT 1	NORMAL RANGE FOR AGE	PATIENT 3	NORMAL RANGE FOR AGE	PATIENT 4	NORMAL RANGE FOR AGE	PATIENT 5	NORMAL RANGE FOR AGE	PATIENT 6	NORMAL RANGE FOR AGE
Hemoglobin (g/dL)	***13.5***	10.6-13.2	***6.5***	11.2-15.7	12.4	10.7-13.4	11.5	11.5-15.5	***12.2***	13.7-17.5
WBC (cells/mL)	3840	4270-11400	4400	3980-10040	14550	4310-11000	8060	3400-9600	5590	4230-9070
Platelets (x10^3 cells/mL)	304	199-367	***569***	173-369	***454***	206-369	***587***	162-380	212	161-347
Total lymphocytes (cells/mL)	***840***	1160-4280	***640***	1180-3740	1400	960-3960	637	480-4900	1040	1320-3570
CD4+ lymphocytes	***108***	334-1556	***188***	334-1556	348	334-1556	***173***	362-1275	***280***	334-1556
CD8+ lymphocytes	440	149-787	173	149-787	199	149-787	***184***	344-911	260	149-787
CD19+ lymphocytes	***0****	81-493	321	81-493	370	81-493	150	49-424	469	81-493
CD16+CD56+ lymphocytes	108	109-607	***30***	109-607	153	109-607	183	87-505	***21***	109-607
Neutrophils (cells/mL)	2390	1640-7870	3370	1560-6130	***12310***	1630-7550	7061	1290-7500	4230	1780-5380
Monocytes (cells/mL)	568	190-810	380	240-860	680	190-850	242	0-1150	***140***	300-820
CRP (mg/L)	***56***	<5.0	***28.6***	<5.0	***22***	<5.0	***56.8***	<5.0	***21.5***	<5.0
ESR (mm/h)	***40***	<20	***114***	<20	***36***	<20	***107***	<20	***73***	<20

Absolute values are displayed. The normal ranges for the age at the time of blood draw are depicted. *Patient treated with rituximab, which ablates B cells

Supplementary Table S3: Autopsy findings in Patient 2

ABNORMAL ORGANS AND TISSUES	FINDINGS
BRAIN	Small, scattered white matter hemorrhagic necrosis, suggestive of systemic microembolic disorder; basal ganglia vascular calcification
HEART	Mild hypertrophy of myocardial muscle fibers and mild intimal thickening of coronary arteries; thickening of the intima and myxoid changes in the media of aorta; pericardial effusion
LUNGS	Diffuse emphysema of the lungs, predominantly in the right middle and lower lobes as well as left lower lobe; large areas of the lung show marked interstitial fibrosis, enclosing mucin lakes and scattered chronic inflammatory infiltrate; areas with loss of lung parenchyma; marked intra-alveolar proteinaceous exudate, foamy macrophages, occasional giant cells, mucus gland hypertrophy in bronchioles and scattered foci of acute bronchopneumonia; marked intimal thickening of small and medium sized pulmonary arteries, especially prominent in the areas of interstitial fibrosis; multiple small nests of neuroendocrine cells
GASTROINTESTINAL TRACT	Suggestion of increased collagen in the submucosa of both small and large bowel; pancreatic acini are dilated and the ducts show thickening with hyalinization.
LIVER	Marked liver congestion with areas of centrilobular necrosis, cholestasis in minor bile ducts and canaliculi, mild fatty change, thickened collagen surrounding small hepatic arteries
KIDNEYS	Widespread coagulative necrosis of the proximal collecting tubules, and granular casts in the distal tubules; entirely infarcted cortex; presence of microthrombi in many glomeruli, consistent with acute tubular necrosis. Focal calcification between proximal tubules; occasional glomerular sclerosis; thickening of the intima of both large and medium-sized arteries.
LYMPHNODES	Enlarged paratracheal lymphnodes with paucity of germinal centers and decreased population of lymphocytes

Supplementary Table S4: Genetic databases and prediction models

Mutations	Chromosome Location	dbSNP 137	ESP 6500	GERP score	MutationTaster	Sift score	Sift prediction	Polyphen2 score	Polyphen2 prediction
V147L	chr5:138,860,456	0	0	-5.83	Polymorphism	0.49	Tolerated	0.007	Benign
N154S	chr5:138,860,434	0	0	3.40	Disease Causing	0.00	Damaging	0.988	Probably Damaging
V155M	chr5:138,860,432	0	0	3.70	Disease Causing	0.00	Damaging	0.999	Probably Damaging

None of the six patients presented with any of the reported single nucleotide polymorphisms (SNPs) in exon 5 of the *TMEM173* gene (rs200049390, rs11554779, rs138074216 and rs184755982).

Supplementary Table S5: Serum cytokine analysis from SAVI patients, healthy controls and NOMID patients

CYTOKINE	SAVI (n=3)	HEALTHY CONTROLS (n=11)	NOMID (n=5)	p-value SAVI vs. HEALTHY CONTROLS	p-value SAVI vs. NOMID	p-value NOMID vs. HEALTHY CONTROLS
IP-10/CXCL10	10331 ± 1941	1434 ± 183.8	2481 ± 563.9	***< 0.0001****	***0.0027****	***0.0382****
GROα/CXCL1	246.4 ± 105.5	76.27 ± 17.14	183.6 ± 55.97	***0.0140****	0.5798	***0.0299****
MIG/CXCL9	1070 ± 351.0	492.2 ± 63.57	1668 ± 480.8	***0.0182****	0.4195	***0.0042****
IL-18	128.8 ± 18.40	78.95 ± 9.536	862.1 ± 218.3	***0.0326****	**0.0455***	***< 0.0001****
VEGF	283.7 ± 65.98	134.8 ± 15.99	348.7 ± 112.5	***0.0053****	0.6942	***0.0142****
IL-2Ra	148.8 ± 18.95	115.1 ± 19.51	803.0 ± 88.04	0.4093	***0.0015****	***< 0.0001****
MIP-1β/CCL4	104.9 ± 26.44	152.7 ± 16.62	157.3 ± 14.95	0.1969	0.1077	0.8644
MCP-1/CCL2	49.62 ± 13.81	37.34 ± 3.246	124.9 ± 68.28	0.1986	0.4427	0.0681
RANTES/CCL5	18813 ± 2075	20390 ± 1411	43218 ± 25605	0.6020	0.5020	0.1918
M-CSF	35.49 ± 27.86	8.631 ± 1.871	55.48 ± 13.49	0.0673	0.4895	***0.0002****
TNF-α	63.48 ± 11.44	81.20 ± 5.673	151.6 ± 67.36	0.1773	0.3664	0.1342
IL-17	59.18 ± 14.59	92.89 ± 11.98	119.5 ± 46.43	0.1949	0.3743	0.4602
IFN-γ	260.1 ± 70.65	346.1 ± 30.44	694.1 ± 359.4	0.2321	0.4026	0.1628
IL-6	29.23 ± 7.963	22.62 ± 1.977	94.74 ± 32.70	0.2403	0.1870	***0.0044****
IL-4	6.395 ± 0.6991	7.489 ± 0.4929	12.11 ± 5.346	0.3063	0.4545	0.2112
IL-2	26.35 ± 2.631	33.17 ± 3.490	58.17 ± 22.06	0.3485	0.3218	0.1215
IL-1Ra	320.2 ± 22.07	378.1 ± 36.41	1358 ± 393.3	0.4402	0.0952	***0.0020****
IL-12p70	105.3 ± 43.33	86.22 ± 9.035	134.7 ± 48.60	0.4888	0.6979	0.1779
IL-7	13.71 ± 4.898	13.47 ± 1.702	71.84 ± 47.25	0.9537	0.3924	0.0769

Results are expressed in Mean ± SEM.
* denotes statistically significant
The following proteins were below the detection limit: TNFβ, SCGFβ, βNGF, MIF, MCP-3, LIF, IFNα2, HGF, IL-16, IL-12p40, IL-3, IL-1α.
The following proteins were measured and did not show significant differences from controls: TRAIL, SCF, CTACK, IL-8, IL-9, eotaxin, FGF, G-CSF, GM-CSF, MCP-1, PDGFβ.